INTERNATIONAL JOURNAL FOR NUMERICAL METHODS IN FLUIDS
Int. J. Numer. Meth. Fluids 2000; **32**: 921–957

Numerical methods for conjunctive two-dimensional surface and three-dimensional sub-surface flows

Masaru Morita[a,*] and Ben Chie Yen[b]

[a] *Department of Civil Engineering, Shibaura Institute of Technology, Minato-ku, Tokyo 108-8548, Japan*
[b] *Department of Civil Engineering, University of Illinois at Urbana-Champaign, Urbana, IL 61801, U.S.A.*

SUMMARY

Sophisticated catchment runoff problems necessitate conjunctive modeling of overland flow and sub-surface flow. In this paper, finite difference numerical methods are studied for simulation of catchment runoff of two-dimensional surface flow interacting with three-dimensional unsaturated and saturated sub-surface flows. The equations representing the flows are mathematically classified as a type of heat diffusion equation. Therefore, two- and three-dimensional numerical methods for heat diffusion equations were investigated for applications to the surface and sub-surface flow sub-models in terms of accuracy, stability, and calculation time. The methods are the purely explicit method, Saul'yev's methods, the alternating direction explicit (ADE) methods, and the alternating direction implicit (ADI) methods. The methods are first examined on surface and sub-surface flows separately; subsequently, 12 selected combinations of methods were investigated for modeling the conjunctive flows. Saul'yev's downstream (S-d) method was found to be the preferred method for two-dimensional surface flow modeling, whereas the ADE method of Barakat and Clark is a less accurate, stable alternative. For the three-dimensional sub-surface flow model, the ADE method of Larkin (ADE-L) and Brian's ADI method are unconditionally stable and more accurate than the other methods. The calculations of the conjunctive models utilizing the S-d surface flow sub-model give excellent results and confirm the expectation that the errors of the surface and sub-surface sub-models interact. The surface sub-model dominates the accuracy and stability of the conjunctive model, whereas the sub-surface sub-model dominates the calculation time, suggesting the desirability of using a smaller time increment for the surface sub-model. Copyright © 2000 John Wiley & Sons, Ltd.

KEY WORDS: conjunctive flow model; heat diffusion equation; surface flow; sub-surface flow; transient flow

1. INTRODUCTION

Many hydraulic and hydrologic problems, including those of urban storm drainage and watershed runoff, involve interaction of flows on the land surface and in the sub-surface

* Correspondence to: Department of Civil Engineering, Shibaura Institute of Technology, 3-9-14 Shibaura, Minato-ku, Tokyo 108-8548, Japan.

Received 29 October 1997
Revised 18 May 1999

porous media. Numerical modeling of such conjunctive surface–sub-surface flows involves three components: (i) the sub-surface flow partial differential equation (PDE), which is of the parabolic type; (ii) the surface flow PDE, which is either of the hyperbolic or parabolic type; and (iii) coupling of the surface and sub-surface flows through the common internal boundary condition of infiltration through the interface between the surface and sub-surface media.

There are three different ways to connect these components for conjunctive numerical simulation. The simplest and least accurate way is the uncoupled model of solving the surface flow sub-model and sub-surface flow sub-model separately in succession without iteration. A simple infiltration rate expression is used as the common boundary condition between the sub-models. Freeze [1] called this uncoupled conjunctive approach 'externally coupled'. The surface flow model is usually solved first because of the relatively short runoff period and the rapid change of flow. The result is passed on to solve the sub-surface flow at the same time step before advancing to solve the surface flow at the next time step. In simulation, the discretization time scale used for the sub-surface flow is often much larger than that for the surface flow [1–3]. Smith and Woolhiser [4] were the first to publish on conjunctive surface–sub-surface flow simulation using this type of uncoupled modeling. They used the Lax–Wendroff second-order explicit scheme to solve a hyperbolic-type PDE of one-dimensional kinematic wave overland flow and the non-linear Crank–Nicolson implicit scheme to solve a parabolic-type PDE of one-dimensional (vertical) single-phase flow in the unsaturated sub-surface medium. Liggett and Dillon [2] used the conjunctive but uncoupled approach by solving the one-dimensional unsaturated sub-surface flow using the boundary integral equation method (BIEM) conjunctively with one-dimensional channel flow Muskingum–Cunge kinematic wave routing. A simplified variation of this uncoupled approach is to express the vertically downward one-dimensional sub-surface flow as an algebraic equation instead of a PDE. This approach is popular in border irrigation studies. For example, Katopodes and Strelkoff [5] and Playan *et al*. [6] used the Kostiakov infiltration equation. The US Department of Agriculture WEPP model [7] used the Green–Ampt infiltration formula. Singh and Bhallamudi [8] allowed a choice of the Kostiakov equation or the quasi-analytical Parlange equation for the infiltration calculation.

The second way to join the conjunctive flow components together is coupled modeling for which the surface and sub-surface sub-models are solved separately but iteratively at the same time step joined by a gradient-type equation, representing the infiltration as the common internal boundary between the two sub-models. Solutions for surface and sub-surface flows at a time step are achieved when the iterative errors are within specified acceptable tolerances before advancing to the next time step.

The third way of conjunctive modeling is a coupled model in which the surface flow equation, sub-surface flow equation, and common internal boundary condition of an infiltration equation are all solved as simultaneous equations at a time step before advancing to the next time step. No study has been reported in the literature on the third way for the solution. Numerically, the first way is the simplest, whereas the third way is the most sophisticated and theoretically the most satisfactory approach. For future reference, the first way is referred to as an uncoupled model, the second way is referred to as an alternating iterative model, whereas the third way is referred to as a coupled simultaneous solution model.

Pinder and Sauer [9] were the first to report on a coupled alternating iterative model. They used a staggered explicit scheme to solve the hyperbolic-type differential equation of one-dimensional channel flow conjunctively with an alternating direction implicit (ADI) method for the two-dimensional saturated groundwater flow parabolic-type PDE, coupled iteratively through a gradient-type infiltration equation as the common internal boundary condition. Akan and Yen [10] developed a coupled alternating iterative conjunctive model for one-dimensional overland surface flow and two-dimensional sub-surface flow. A four-point implicit scheme was applied to solve the hyperbolic-type unsteady, overland flow, dynamic wave equations. A successive line overrelaxation implicit scheme was applied to solve the non-linear parabolic-type PDE of two-dimensional flow in unsaturated and/or saturated porous media. The coupling was achieved through infiltration at the ground surface considering conservation and pressure relationship as the common internal boundary condition using a quasi-implicit iterative scheme. Schmitz *et al.* [11] used an approximate quasi-analytic Parlange infiltration equation for one-dimensional (vertical) sub-surface flow coupled iteratively with one-dimensional overland flow, dynamic wave equations solved by using an implicit method of characteristics. Freeze [1] formulated a conjunctive model using the Lax–Wendroff explicit scheme to solve the one-dimensional channel flow dynamic wave, hyperbolic-type equations and a successive line overrelaxation technique to solve the three-dimensional unsaturated sub-surface flow, non-linear, parabolic-type equation. The model was formulated to allow coupled alternating iterative simulation, but the results presented were obtained without iteration as in an uncoupled conjunctive model.

For practical reasons it is desirable to extend the coupled conjunctive model to two-dimensional surface and three-dimensional sub-surface flow models to deal with two-dimensional surface flow and three-dimensional sub-surface flow, because various kinds of infiltration facilities for urban storm drainage, stream-bed infiltration, and porous-bed storage ponds need more accurate analyses than the one-dimensional surface and one- or two-dimensional sub-surface flow simulation. In this paper, finite difference numerical methods are studied for coupled alternating iterative simulation modeling of the two-dimensional surface flow conjunctive with three-dimensional sub-surface flow. The equations representing both flows are mathematically classified as a type of heat diffusion equation. Therefore, two- and three-dimensional numerical methods for heat diffusion equations can be applied to solve the flow equations. Numerical schemes of the purely explicit method, alternating direction explicit (ADE) methods, and alternating direction implicit (ADI) methods are investigated for application to the surface and sub-surface flow sub-models in terms of accuracy, stability, and calculation time. The conjunctive model coupling calculations are examined.

2. GOVERNING EQUATIONS

In the present study, the non-inertia unsteady flow equations (inappropriately named diffusion wave equations in some hydraulic literature) for two-dimensional surface flow and the Richards equation for three-dimensional sub-surface flow are applied. The conjunctive flow model simulates the interaction between the surface and sub-surface flows and the solution is obtained numerically. The theoretical formulation of the conjunctive model is not presented

here, but is described in a companion paper [Morita M, Yen BC. Modeling of conjunctive 2D surface 3D subsurface flows. *Journal of Hydraulic Engineering*, *ASCE*, submitted].

2.1. Surface flow

The continuity equation and momentum equation in the non-inertia approximation for two-dimensional surface flow on an x–y overland plane can be combined to yield the governing equation for the surface flow as

$$\frac{\partial H_s}{\partial t} = \frac{\partial}{\partial x} D_x \frac{\partial H_s}{\partial x} + \frac{\partial}{\partial y} D_y \frac{\partial H_s}{\partial y} + r - i \tag{1}$$

where H_s is the elevation of the free surface, r is the rainfall intensity, i is the infiltration rate, and D_x and D_y are described by

$$(D_x, D_y) = \left(\sqrt{\frac{8gh^3}{f_d}} \left| \frac{\partial H_s}{\partial x} \right|^{-1/2}, \sqrt{\frac{8gh^3}{f_d}} \left| \frac{\partial H_s}{\partial y} \right|^{-1/2} \right) \tag{2}$$

where h is the flow depth, $h = H_s -$ bed elevation; f_d is the Weisbach resistance coefficient, which is a function of the Reynolds number, $Re = vh/\nu$, in which ν is the kinematic viscosity of the fluid and v is the flow velocity, $v = (v_x^2 + v_y^2)^{1/2}$, with $v_x = -(D_x/h)(\partial H_s/\partial x)$, $v_y = -(D_y/h)(\partial H_s/d_y)$.
For laminar flow having $Re < 500$

$$f_d = 24/Re \tag{3}$$

For transitional flow with $500 < Re < 30\,000$

$$f_d = 0.223/Re^{0.25} \tag{4}$$

For turbulent flow with $Re > 30\,000$ and $k_s/R < 0.05$ [12],

$$f_d = \frac{1}{4}\left[-\log\left(\frac{k_s}{12R} + \frac{1.95}{Re^{0.9}} \right) \right]^{-2} \tag{5}$$

where k_s is the equivalent sand-grain roughness size, and R is the hydraulic radius equal to h for overland flow.

Equation (1) can be written in non-dimensional form in a simple way [13],

$$\frac{\partial H_s^*}{\partial t^*} = \left(\frac{D_r t_r}{x_r^2} \right) \frac{\partial}{\partial x^*} D_x^* \frac{\partial H_s^*}{\partial x^*} + \left(\frac{D_r t_r}{x_r^2} \right) \left(\frac{x_r^2}{y_r^2} \right) \frac{\partial}{\partial y^*} D_y^* \frac{\partial H_s^*}{\partial y^*} + \left(\frac{r_r t_r}{H_{sr}} \right) r^* + \left(\frac{i_r t_r}{H_{sr}} \right) i^* \tag{6}$$

in which $H_s^* = H_s/H_{sr}$; $t^* = t/t_r$; $x^* = x/x_r$; $y^* = y/y_r$; $D_x^* = D_x/D_r$; $D_y = D_y/D_r$; $r^* = r/r_r$; and $i = i/i_r$; H_{sr}, t_r, x_r, y_r, D_r, r_r and i_r are the reference values of H_s, t, x, y, D_x, D_y, r and i respectively.

If Equation (1) is completely linear with constant D_x and D_y, Equation (6) can be simplified as

$$\frac{\partial H_s^*}{\partial t^*} = \frac{\partial^2 H_s^*}{\partial x^{*2}} + \frac{\partial^2 H_s^*}{\partial y^{*2}} + r^* - i^* \tag{7}$$

For this equation, the relations of the reference values of $D_x = D_y = D_r$, $D_r t_r / x_r^2 = 1$, $x_r = y_r$, $r_r t_r / H_{sr} = 1$, and $i_r t_r / H_{sr} = 1$, are used.

2.2. Sub-surface flow

The three-dimensional sub-surface flow is represented by the Richards equation [1,10],

$$\frac{\partial H}{\partial t} = \frac{\partial}{\partial x}\alpha_x(\theta)\frac{\partial H}{\partial x} + \frac{\partial}{\partial y}\alpha_y(\theta)\frac{\partial H}{\partial y} + \frac{\partial}{\partial z}\alpha_z(\theta)\frac{\partial H}{\partial z} \tag{8}$$

$$\alpha_i(\theta) = K_{si} K_R / (\partial\theta / \partial P) \tag{9}$$

where H is the piezometric head; α_x, α_y and α_z are the moisture diffusivity coefficients in the x-, y- and z-directions respectively; K_{sx}, K_{sy} and K_{sz} are the saturated hydraulic conductivities in the x-, y- and z-directions respectively; K_R is the relative hydraulic conductivity; P is the capillary pressure head; θ is the volumetric moisture content ($\theta = nS$, where n is the soil porosity and S is the saturation degree). The soil hydraulic conductivity is $K_i = K_{si} K_R$. The piezometric head H is related to P by $H = P + z$.

Equation (8) can be applied to both saturated groundwater flow and unsaturated soil water flow. For saturated flow, P is positive and K_R is equal to unity. In the calculation of unsaturated flow, the relation among P, S and K_R is used for the non-linear Equation (8). This P–S–K_R relation is assumed to be constant in time without a hysteresis effect in the present study.

In the same way as for the surface flow equation, Equation (8) can be non-dimensionalized as

$$\frac{\partial H^*}{\partial t^*} = \left(\frac{\alpha_r t_r}{x_r^2}\right)\frac{\partial}{\partial x^*}\alpha_x^*\frac{\partial H^*}{\partial x^*} + \left(\frac{\alpha_r t_r}{x_r^2}\right)\left(\frac{x_r^2}{y_r^2}\right)\frac{\partial}{\partial y^*}\alpha_y^*\frac{\partial H^*}{\partial y^*} + \left(\frac{\alpha_r t_r}{x_r^2}\right)\left(\frac{x_r^2}{z_r^2}\right)\frac{\partial}{\partial z^*}\alpha_z^*\frac{\partial H^*}{\partial z^*} \tag{10}$$

where $H^* = H/H_r$; $t^* = t/t_r$; $x^* = x/x_r$; $y^* = y/y_r$; $z^* = z/z_r$; $\alpha_x = \alpha_x/\alpha_r$; $\alpha_y = \alpha_y/\alpha_r$; and $\alpha_z = \alpha_z/\alpha_r$; H_r, t_r, x_r, y_r, z_r and α_r are the reference values of H, t, x, y, z, α_x, α_y and α_z respectively.

In a similar way as that in introducing Equation (7), Equation (11) can be obtained for a complete linear case

$$\frac{\partial H^*}{\partial t^*} = \frac{\partial^2 H^*}{\partial x^{*2}} + \frac{\partial^2 H^*}{\partial y^{*2}} + \frac{\partial^2 H^*}{\partial z^{*2}} \tag{11}$$

For Equation (11), the reference values have the relations of $x_r = y_r = z_r$, $\alpha_r t_r / x_r^2 = 1$, and $\alpha_x^* = \alpha_y^* = \alpha_z^* = 1$.

2.3. Coupling of surface and sub-surface flow models

As mentioned previously in Section 1, in this study a coupled alternating iterative solution model for the two-dimensional surface flow described by Equation (1) interacting with the three-dimensional sub-surface flow described by Equation (8) is considered. For coupling the surface and sub-surface flow sub-models together, the supply from rainfall is compared first with the demand of potential infiltration capacity, or infiltrability, I_p, for simplicity, to determine the actual infiltration rate i for each time step as shown schematically in Figure 3,

$$i = -0.5(K_s + K_1)(H_1 - H_0)/\Delta z \tag{12}$$

where K_1, and H_1 are the soil hydraulic conductivity and piezometric head at the first node in the z-direction measured from the overland surface, and H_0 is the surface piezometric head, which is the common boundary condition. The procedure is repeated until the surface and sub-surface flow solutions change within a specified acceptable tolerance. Then the computations advance to the next time step. Actually, one cycle of iteration is usually sufficient owing to the slow response of the sub-surface flow to the surface flow depth variation.

3. NUMERICAL METHODS FOR SURFACE AND SUB-SURFACE FLOWS

Numerous numerical methods have been proposed and published to solve two- and three-dimensional flow problems. No comprehensive and systematic study has been published to evaluate and compare these methods. Thibault [14] investigated nine commonly known three-dimensional finite difference methods for solving the heat diffusion equation. His results are useful for the selection of the numerical methods for solving the three-dimensional sub-surface flow and two-dimensional surface flow equations. Thibault demonstrated that the direct implicit method of solving the set of algebraic equations of the three dimensions simultaneously and a Crank–Nicolson formulation are prohibitively demanding in computer time. Based on Thibault's results and information available from the literature on methods well known to engineers and scientists (e.g. Anderson *et al.* [15]), in this study five numerical methods are investigated for the three-dimensional sub-surface flow and six numerical methods are investigated for the two-dimensional surface flow. From the results of these investigations, four surface flow models were coupled with three sub-surface flow models to test conjunctive flow modeling. Other more sophisticated three- and two-dimensional numerical methods are available, but are not studied here. For example, the conjugate gradients (CG) preconditioning method has been successfully applied to accelerate the convergence of iterative procedures for boundary value problems [16]; and the arbitrary meshes multigrid method [17] and the Jameson [18] Runge–Kutta multi-stage time integration method have also been developed to accelerate the convergence of transonic potential flow calculation. These new methods could be applied to more complicated and sophisticated surface and sub-surface flow problems and an investigation in the future on their applications is in order.

3.1. Sub-surface flow

For three-dimensional sub-surface flow modeling, five numerical methods have been chosen for testing as shown in Table I. The computational co-ordinate system is shown in Figure 1, where infiltration from surface water is mainly through the interface ABCD downward. The moisture diffusivity coefficient $\alpha_i(\theta)$ in Equation (8) is discretized as given in Table II.

Among the five methods, three of them are of the explicit type: purely explicit, ADE of Barakat and Clark [19], and ADE of Larkin [20]. The other two are of the implicit type: purely ADI and ADI of Brian [21].

Larkin's ADE method is actually a modification of Saul'yev's [22] method. It is an explicit method and also an alternating direction method, because the governing equation is solved independently in the downward direction for U by Saul'yev's downstream method and in the upward direction for V by Saul'yev's upstream method. After these calculations, the two results, U and V, are averaged to yield one solution of H at each time step. The word 'downstream' or 'upstream' used in Saul'yev's method refers to the directions, $A \rightarrow G$ and $G \rightarrow A$ in Figure 1 respectively. Barakat and Clark's ADE method is also a modification of Saul'yev's method and differs slightly from that of Larkin. Barakat and Clark used two intermediate values of U and V to calculate H at the next time level as described in Table I.

The purely ADI method is a three-dimensional ADI method extended from the two-dimensional ADI method by Peaceman and Rachford [23]. Brian's [21] ADI method is developed from the three-dimensional purely ADI method modified for the three-dimensional heat diffusion equation considering the stability problem. ADI methods solve simultaneous equations implicitly and usually require more calculation time than the explicit methods.

3.2. Surface flow

Numerical methods considered for surface flow and their discretization schemes are shown in Table III. Five of the six numerical methods applied here are explicit schemes: the purely explicit method, Saul'yev's [22] downstream method, Saul'yev's upstream method, Larkin's [20] ADE method, and Barakat and Clark's [19] ADE method. The ADI method applied here has an implicit alternating direction scheme and is identical with the Peaceman and Rachford [23] ADI method. The schematic diagram of the tested surface flow and computation grid is shown in Figure 2. The word 'downstream' and 'upstream' used in Saul'yev's method refers to the directions shown in Figure 2.

4. COMPARISON OF NUMERICAL METHODS FOR SURFACE FLOW

The comparison between calculated values and experimental data provides useful information on the applicability of the numerical methods studied. Before investigating the two-dimensional surface flow model in terms of stability, accuracy and calculation time, a set of published physical experimental data obtained by Izzard [24] was preliminarily compared with the numerically calculated results of the six numerical methods. Izzard's experimental plot was 72 ft long, 6 ft wide, and had a bed slope of 0.001. The surface was covered with crushed slate roofing paper. Surface runoff was produced by simulated uniform rainfall over the entire plot

Table I. Discretization in the numerical methods for sub-surface flow.

Basic equation	$\frac{\partial H}{\partial t}=\frac{\partial}{\partial x}\alpha_x\frac{\partial H}{\partial x}+\frac{\partial}{\partial y}\alpha_y\frac{\partial H}{\partial y}+\frac{\partial}{\partial z}\alpha_z\frac{\partial H}{\partial z}$
Purely explicit method	$\frac{H^{t+\Delta t}_{i,j,k}-H^t_{i,j,k}}{\Delta t}=\frac{\alpha_{x1}}{(\Delta x)^2}(H^t_{i-1,j,k}-H^t_{i,j,k})+\frac{\alpha_{x2}}{(\Delta x)^2}(H^t_{i+1,j,k}-H^t_{i,j,k})$ $+\frac{\alpha_{y1}}{(\Delta y)^2}(H^t_{i,j-1,k}-H^t_{i,j,k})+\frac{\alpha_{y2}}{(\Delta y)^2}(H^t_{i,j+1,k}-H^t_{i,j,k})$ $+\frac{\alpha_{z1}}{(\Delta z)^2}(H^t_{i,j,k-1}-H^t_{i,j,k})+\frac{\alpha_{z2}}{(\Delta z)^2}(H^t_{i,j,k+1}-H^t_{i,j,k})$
ADE method of Barakat and Clark [19]	$\frac{U^{t+\Delta t}_{i,j,k}-U^t_{i,j,k}}{\Delta t}=\frac{\alpha_{x1}}{(\Delta x)^2}(U^{t+\Delta t}_{i-1,j,k}-U^{t+\Delta t}_{i,j,k})+\frac{\alpha_{x2}}{(\Delta x)^2}(U^t_{i+1,j,k}-U^t_{i,j,k})$ $+\frac{\alpha_{y1}}{(\Delta y)^2}(U^{t+\Delta t}_{i,j-1,k}-U^{t+\Delta t}_{i,j,k})+\frac{\alpha_{y2}}{(\Delta y)^2}(U^t_{i,j+1,k}-U^t_{i,j,k})$ $+\frac{\alpha_{z1}}{(\Delta z)^2}(U^{t+\Delta t}_{i,j,k-1}-U^{t+\Delta t}_{i,j,k})+\frac{\alpha_{z2}}{(\Delta z)^2}(U^t_{i,j,k+1}-U^t_{i,j,k})$ $\frac{V^{t+\Delta t}_{i,j,k}-V^t_{i,j,k}}{\Delta t}=\frac{\alpha_{x1}}{(\Delta x)^2}(V^t_{i-1,j,k}-V^t_{i,j,k})+\frac{\alpha_{x2}}{(\Delta x)^2}(V^{t+\Delta t}_{i+1,j,k}-V^{t+\Delta t}_{i,j,k})$ $+\frac{\alpha_{y1}}{(\Delta y)^2}(V^t_{i,j-1,k}-V^t_{i,j,k})+\frac{\alpha_{y2}}{(\Delta y)^2}(V^{t+\Delta t}_{i,j+1,k}-V^{t+\Delta t}_{i,j,k})$ $+\frac{\alpha_{z1}}{(\Delta z)^2}(V^t_{i,j,k-1}-V^t_{i,j,k})+\frac{\alpha_{z2}}{(\Delta z)^2}(V^{t+\Delta t}_{i,j,k+1}-V^{t+\Delta t}_{i,j,k})$ $H^{t+\Delta t}_{i,j,k}=\frac{U^{t+\Delta t}_{i,j,k}+V^{t+\Delta t}_{i,j,k}}{2}$
ADE method of Larkin [20]	$\frac{U^{t+t\Delta t}_{i,j,k}-H^t_{i,j,k}}{\Delta t}=\frac{\alpha_{x1}}{(\Delta x)^2}(U^{t+\Delta t}_{i-1,j,k}-U^{t+\Delta t}_{i,j,k})+\frac{\alpha_{x2}}{(\Delta x)^2}(H^t_{i+1,j,k}-H^t_{i,j,k})$ $+\frac{\alpha_{y1}}{(\Delta y)^2}(U^{t+\Delta t}_{i,j-1,k}-U^{t+\Delta t}_{i,j,k})+\frac{\alpha_{y2}}{(\Delta y)^2}(H^t_{i,j+1,k}-H^t_{i,j,k})$ $+\frac{\alpha_{z1}}{(\Delta z)^2}(U^{t+\Delta t}_{i,j,k-1}-U^{t+\Delta t}_{i,j,k})+\frac{\alpha_{z2}}{(\Delta z)^2}(H^t_{i,j,k+1}-H^t_{i,j,k})$ $\frac{V^{t+t\Delta t}_{i,j,k}-H^t_{i,j,k}}{\Delta t}=\frac{\alpha_{x1}}{(\Delta x)^2}(H^t_{i-1,j,k}-H^t_{i,j,k})+\frac{\alpha_{x2}}{(\Delta x)^2}(V^{t+\Delta t}_{i+1,j,k}-V^{t+\Delta t}_{i,j,k})$ $+\frac{\alpha_{y1}}{(\Delta y)^2}(H^t_{i,j-1,k}-H^t_{i,j,k})+\frac{\alpha_{y2}}{(\Delta y)^2}(V^{t+\Delta t}_{i,j+1,k}-V^{t+\Delta t}_{i,j,k})$ $+\frac{\alpha_{z1}}{(\Delta z)^2}(H^t_{i,j,k-1}-H^t_{i,j,k})+\frac{\alpha_{z2}}{(\Delta z)^2}(V^{t+\Delta t}_{i,j,k+1}-V^{t+\Delta t}_{i,j,k})$ $H^{t+\Delta t}_{i,j,k}=\frac{U^{t+\Delta t}_{i,j,k}+V^{t+\Delta t}_{i,j,k}}{2}$

Table I. (Continued)

Basic equation	$\dfrac{\partial H}{\partial t}=\dfrac{\partial}{\partial x}\alpha_x\dfrac{\partial H}{\partial x}+\dfrac{\partial}{\partial y}\alpha_y\dfrac{\partial H}{\partial y}+\dfrac{\partial}{\partial z}\alpha_z\dfrac{\partial H}{\partial z}$
Purely ADI method	$\dfrac{H^{t+1/3\Delta t}_{i,j,k}-H^{t}_{i,j,k}}{\Delta t/3}=\dfrac{\alpha_{x1}}{(\Delta x)^2}(H^{t+1/3\Delta t}_{i-1,j,k}-H^{t+1/3\Delta t}_{i,j,k})+\dfrac{\alpha_{x2}}{(\Delta x)^2}(H^{t+1/3\Delta t}_{i+1,j,k}-H^{t+1/3\Delta t}_{i,j,k})$ $+\dfrac{\alpha_{y1}}{(\Delta y)^2}(H^{t}_{i,j-1,k}-H^{t}_{i,j,k})+\dfrac{\alpha_{y2}}{(\Delta y)^2}(H^{t}_{i,j+1,k}-H^{t}_{i,j,k})$ $+\dfrac{\alpha_{z1}}{(\Delta z)^2}(H^{t}_{i,j,k-1}-H^{t}_{i,j,k})+\dfrac{\alpha_{z2}}{(\Delta z)^2}(H^{t}_{i,j,k+1}-H^{t}_{i,j,k})$
	$\dfrac{H^{t+2/3\Delta t}_{i,j,k}-H^{t+1/3\Delta t}_{i,j,k}}{\Delta t/3}=\dfrac{\alpha_{x1}}{(\Delta x)^2}(H^{t+1/3\Delta t}_{i-1j,k}-H^{t+1/3\Delta t}_{i,j,k})+\dfrac{\alpha_{x2}}{(\Delta x)^2}(H^{t+1/3\Delta t}_{i+1,j,k}-H^{t+1/3\Delta t}_{i,j,k})$ $+\dfrac{\alpha_{y1}}{(\Delta y)^2}(H^{t+2/3\Delta t}_{i,j-1,k}-H^{t+2/3\Delta t}_{i,j,k})+\dfrac{\alpha_{y2}}{(\Delta y)^2}(H^{t+2/3\Delta t}_{i,j+1,k}-H^{t+2/3\Delta t}_{i,j,k})$ $+\dfrac{\alpha_{z1}}{(\Delta z)^2}(H^{t+1/3\Delta t}_{i,j,k-1}-H^{t+1/3\Delta t}_{i,j,k})+\dfrac{\alpha_{z2}}{(\Delta z)^2}(H^{t+1/3\Delta t}_{i,j,k+1}-H^{t+1/3\Delta t}_{i,j,k})$
	$\dfrac{H^{t+\Delta t}_{i,j,k}-H^{t+2/3\Delta t}_{i,j,k}}{\Delta t/3}=\dfrac{\alpha_{x1}}{(\Delta x)^2}(H^{t+2/3\Delta t}_{i-1,j,k}-H^{t+2/3\Delta t}_{i,j,k})+\dfrac{\alpha_{x2}}{(\Delta x)^2}(H^{t+2/3\Delta t}_{i+1,j,k}-H^{t+2/3\Delta t}_{i,j,k})$ $+\dfrac{\alpha_{y1}}{(\Delta y)^2}(H^{t+2/3\Delta t}_{i,j-1,k}-H^{t+2/3\Delta t}_{i,j,k})+\dfrac{\alpha_{y2}}{(\Delta y)^2}(H^{t+2/3\Delta t}_{i,j+1,k}-H^{t+2/3\Delta t}_{i,j,k})$ $+\dfrac{\alpha_{z1}}{(\Delta z)^2}(H^{t+\Delta t}_{i,j,k-1}-H^{t+\Delta t}_{i,j,k})+\dfrac{\alpha_{z2}}{(\Delta z)^2}(H^{t+\Delta t}_{i,j,k+1}-H^{t+\Delta t}_{i,j,k})$
ADI method of Brian [21]	$\dfrac{U_{i,j,k}-H^{t}_{i,j,k}}{\Delta t/2}=\dfrac{\alpha_{x1}}{(\Delta x)^2}(U_{i-1,j,k}-U_{i,j,k})+\dfrac{\alpha_{x2}}{(\Delta x)^2}(U_{i+1,j,k}-U_{i,j,k})$ $+\dfrac{\alpha_{y1}}{(\Delta y)^2}(H^{t}_{i,j-1,k}-H^{t}_{i,j,k})+\dfrac{\alpha_{y2}}{(\Delta y)^2}(H^{t}_{i,j+1,k}-H^{t}_{i,j,k})$ $+\dfrac{\alpha_{z1}}{(\Delta z)^2}(H^{t}_{i,j,k-1}-H^{t}_{i,j,k})+\dfrac{\alpha_{z2}}{(\Delta z)^2}(H^{t}_{i,j,k+1}-H^{t}_{i,j,k})$
	$\dfrac{V_{i,j,k}-H^{t}_{i,j,k}}{\Delta t/2}=\dfrac{\alpha_{x1}}{(\Delta x)^2}(U_{i-1,j,k}-U_{i,j,k})+\dfrac{\alpha_{x2}}{(\Delta x)^2}(U_{i+1,j,k}-U_{i,j,k})$ $+\dfrac{\alpha_{y1}}{(\Delta y)^2}(V_{i,j-1,k}-V_{i,j,k})+\dfrac{\alpha_{y2}}{(\Delta y)^2}(V_{i,j+1,k}-V_{i,j,k})$ $+\dfrac{\alpha_{z1}}{(\Delta z)^2}(H^{t}_{i,j,k-1}-H^{t}_{i,j,k})+\dfrac{\alpha_{z2}}{(\Delta z)^2}(H^{t}_{i,j,k+1}-H^{t}_{i,j,k})$
	$\dfrac{H^{t+\Delta t}_{i,j,k}-V_{i,j,k}}{\Delta t/2}=\dfrac{\alpha_{x1}}{(\Delta x)^2}(U_{i-1,j,k}-U_{i,j,k})+\dfrac{\alpha_{x2}}{(\Delta x)^2}(U_{i+1,j,k}-U_{i,j,k})$ $+\dfrac{\alpha_{y1}}{(\Delta y)^2}(V_{i,j-1,k}-V_{i,j,k})+\dfrac{\alpha_{y2}}{(\Delta y)^2}(V_{i,j+1,k}-V_{i,j,k})$ $+\dfrac{\alpha_{z1}}{(\Delta z)^2}(H^{t+\Delta t}_{i,j,k-1}-H^{t+\Delta t}_{i,j,k})+\dfrac{\alpha_{z2}}{(\Delta z)^2}(H^{t+\Delta t}_{i,j,k+1}-H^{t+\Delta t}_{i,j,k})$

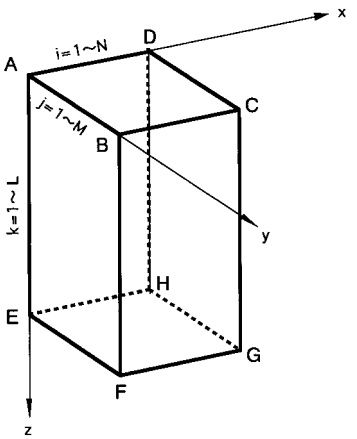

Figure 1. Computational grid sub-surface flow model.

and the discharge Q was measured at the downstream end of the plot. This surface flow was practically one-dimensional. It would be desirable to verify the model by using experimental data of two-dimensional curvilinear flow. However, reliable data of such flow are not available. Therefore, Izzard's plot was set in the computational grid at either 45° or 26.6° to the x-direction (Figure 2) for the verification of the two-dimensional surface flow model. The calculation was thus carried out two-dimensionally as described previously in Section 2. The computed velocity at the downstream end of the plot, v_d, was checked to confirm it was

Table II. Discretization of moisture diffusivity coefficients.

Coefficient	Discretization
α_{x1}	$\dfrac{\frac{1}{2}(K_{i-1,j,k}+K_{i,j,k})}{(\partial\theta/\partial P)_{i,j,k}}=\dfrac{\langle\alpha\rangle_{i,j,k}}{2}\left(1+\dfrac{K_{i-1,j,k}}{K_{i,j,k}}\right)$
α_{x2}	$\dfrac{\frac{1}{2}(K_{i+1,j,k}+K_{i,j,k})}{(\partial\theta/\partial P)_{i,j,k}}=\dfrac{\langle\alpha\rangle_{i,j,k}}{2}\left(1+\dfrac{K_{i+1,j,k}}{K_{i,j,k}}\right)$
α_{y1}	$\dfrac{\frac{1}{2}(K_{i,j-1,k}+K_{i,j,k})}{(\partial\theta/\partial P)_{i,j,k}}=\dfrac{\langle\alpha\rangle_{i,j,k}}{2}\left(1+\dfrac{K_{i,j-1,k}}{K_{i,j,k}}\right)$
α_{y2}	$\dfrac{\frac{1}{2}(K_{i,j+1,k}+K_{i,j,k})}{(\partial\theta/\partial P)_{i,j,k}}=\dfrac{\langle\alpha\rangle_{i,j,k}}{2}\left(1+\dfrac{K_{i,j+1,k}}{K_{i,j,k}}\right)$
α_{z1}	$\dfrac{\frac{1}{2}(K_{i,j,k-1}+K_{i,j,k})}{(\partial\theta/\partial P)_{i,j,k}}=\dfrac{\langle\alpha\rangle_{i,j,k}}{2}\left(1+\dfrac{K_{i,j,k-1}}{K_{i,j,k}}\right)$
α_{z2}	$\dfrac{\frac{1}{2}(K_{i,j,k+1}+K_{i,j,k})}{(\partial\theta/\partial P)_{i,j,k}}=\dfrac{\langle\alpha\rangle_{i,j,k}}{2}\left(1+\dfrac{K_{i,j,k+1}}{K_{i,j,k}}\right)$
$\langle\alpha\rangle_{i,j,k}=K_{i,j,k}/(\partial\theta/\partial P)_{i,j,k}$	

Table III. Discretization in the numerical methods for surface.

Basic equation	$\frac{\partial H}{\partial t}=\frac{\partial}{\partial x}D_x\frac{\partial H}{\partial x}+\frac{\partial}{\partial y}D_y\frac{\partial H}{\partial y}$
Purely explicit method	$\frac{H_{i,j}^{t+\Delta t}-H_{i,j}^{t}}{\Delta t}=\frac{D_{x1}}{(\Delta x)^2}(H_{i-1,j}^{t}-H_{i,j}^{t})+\frac{D_{x2}}{(\Delta x)^2}(H_{i+1,j}^{t}-H_{i,j}^{t})+\frac{D_{y1}}{(\Delta y)^2}(H_{i,j-1}^{t}-H_{i,j}^{t})+\frac{D_{y2}}{(\Delta y)^2}(H_{i,j+1}^{t}-H_{i,j}^{t})$
Saul'yev's method [22] (downstream)	$\frac{U_{i,j}^{t+\Delta t}-U_{i,j}^{t}}{\Delta t}=\frac{D_{x1}}{(\Delta x)^2}(U_{i-1,j}^{t+\Delta t}-U_{i,j}^{t+\Delta t})+\frac{D_{x2}}{(\Delta x)^2}(U_{i+1,j}^{t}-U_{i,j}^{t})+\frac{D_{y1}}{(\Delta y)^2}(U_{i,j-1}^{t+\Delta t}-U_{i,j}^{t+\Delta t})+\frac{D_{y2}}{(\Delta y)^2}(U_{i,j+1}^{t}-U_{i,j}^{t})$
Saul'yev's method [22] (upstream)	$\frac{V_{i,j}^{t+\Delta t}-V_{i,j}^{t}}{\Delta t}=\frac{D_{x1}}{(\Delta x)^2}(V_{i-1,j}^{t}-V_{i,j}^{t})+\frac{D_{x2}}{(\Delta x)^2}(V_{i+1,j}^{t+\Delta t}-V_{i,j}^{t+\Delta t})+\frac{D_{y1}}{(\Delta y)^2}(V_{i,j-1}^{t}-V_{i,j}^{t})+\frac{D_{y2}}{(\Delta y)^2}(V_{i,j+1}^{t+\Delta t}-V_{i,j}^{t+\Delta t})$
ADE method of Barakat and Clark [19]	$H_{i,j}^{t+\Delta t}=\frac{U_{i,j}^{t+\Delta t}+V_{i,j}^{t+\Delta t}}{2}$ U, V computed as in Saul'yev's downstream and upstream methods
ADE method of Larkin [20]	$\frac{U_{i,j}^{t+\Delta t}-H_{i,j}^{t}}{\Delta t}=\frac{D_{x1}}{(\Delta x)^2}(U_{i-1,j}^{t+\Delta t}-U_{i,j}^{t+\Delta t})+\frac{D_{x2}}{(\Delta x)^2}(H_{i+1,j}^{t}-H_{i,j}^{t})+\frac{D_{y1}}{(\Delta y)^2}(U_{i,j-1}^{t+\Delta t}-U_{i,j}^{t+\Delta})+\frac{D_{y2}}{(\Delta y)^2}(H_{i,j+1}^{t}-H_{i,j}^{t})$ $\frac{V_{i,j}^{t+\Delta t}-H_{i,j}^{t}}{\Delta t}=\frac{D_{x1}}{(\Delta x)^2}(H_{i-1,j}^{t}-H_{i,j}^{t})+\frac{D_{x2}}{(\Delta x)^2}(V_{i+1,j}^{t+\Delta t}-V_{i,j}^{t+\Delta t})+\frac{D_{y1}}{(\Delta y)^2}(H_{i,j-1}^{t}-H_{i,j}^{t})+\frac{D_{y2}}{(\Delta y)^2}(V_{i,j+1}^{t+\Delta t}-V_{i,j}^{t+\Delta t})$ $H_{i,j}^{t+\Delta t}=\frac{U_{i,j}^{t+\Delta t}+V_{i,j}^{t+\Delta t}}{2}$
ADI method	$\frac{H_{i,j}^{t+1/2\Delta t}-H_{i,j}^{t}}{\Delta t/2}=\frac{D_{x1}}{(\Delta x)^2}(H_{i-1,j}^{t+1/2\Delta t}-H_{i,j}^{t+1/2\Delta t})+\frac{D_{x2}}{(\Delta x)^2}(H_{i+1,j}^{t+1/2\Delta t}-H_{i,j}^{t+1/2\Delta t})+\frac{D_{y1}}{(\Delta y)^2}(H_{i,j-1}^{t}-H_{i,j}^{t})+\frac{D_{y2}}{(\Delta y)^2}(H_{i,j+1}^{t}-H_{i,j}^{t})$ $\frac{H_{i,j}^{t+\Delta t}-H_{i,j}^{t+1/2\Delta t}}{\Delta t/2}=\frac{D_{x1}}{(\Delta x)^2}(H_{i-1,j}^{t+1/2\Delta t}-H_{i,j}^{t+1/2\Delta t})+\frac{D_{x2}}{(\Delta x)^2}(H_{i+1,j}^{t+1/2\Delta t}-H_{i,j}^{t+1/2\Delta t})+\frac{D_{y1}}{(\Delta y)^2}(H_{i,j-1}^{t+\Delta t}-H_{i,j}^{t+\Delta t})+\frac{D_{y2}}{(\Delta y)^2}(H_{i,j+1}^{t+\Delta t}-H_{i,j}^{t+\Delta t})$

uniform across the width of the surface, b. The discharge Q was computed as $v_d hb$. The data of Izzard's Run 138 was used for the comparison. The calculated results agree excellently with the experimental data.

A comparison of the computed results with analytic solutions, if possible, is a desirable way to evaluate the numerical methods. However, no analytic solution exists for the quasi-linear differential equations of two-dimensional surface runoff. Instead, the steady state discharge resulting from a spatially uniform rainfall with constant intensity for 18 min is compared with the simulated results. After the runoff reaching the equilibrium stage, the computed discharge Q should be identical to the rain input rate, r_c. The discharge after 8 min or 480 s of a constant rain intensity of 90.2 mm h^{-1} on the same plot as Izzard's experiment was calculated using the six different numerical methods studied. In this verification, the value of $(Q - r_c)/r_c$ was used as the relative error. For the surface flow on Izzard's experimental plot, the reference values in the non-dimensional equation (6) are set as follows: $x_r = y_r = L_p/\sqrt{2}$ and $t_r = 480$ s, in which the length of the plot is $L_p = 72$ ft.

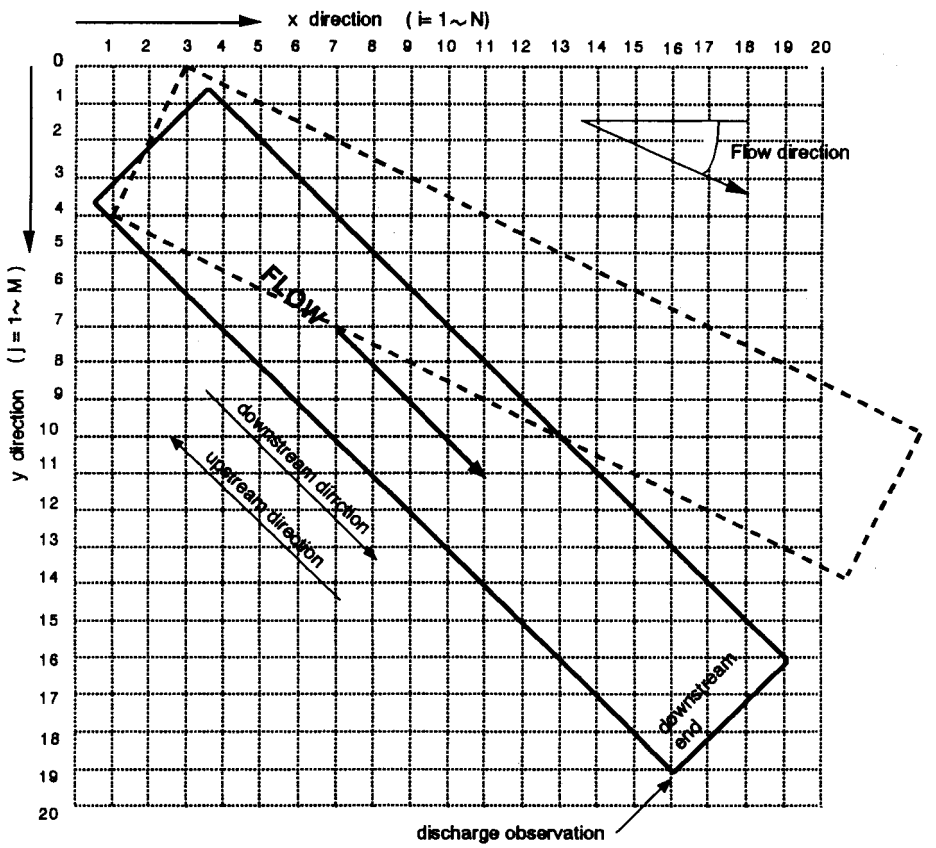

Figure 2. Computational grid for two-dimensional simulation of Izzard's surface flow experiment.

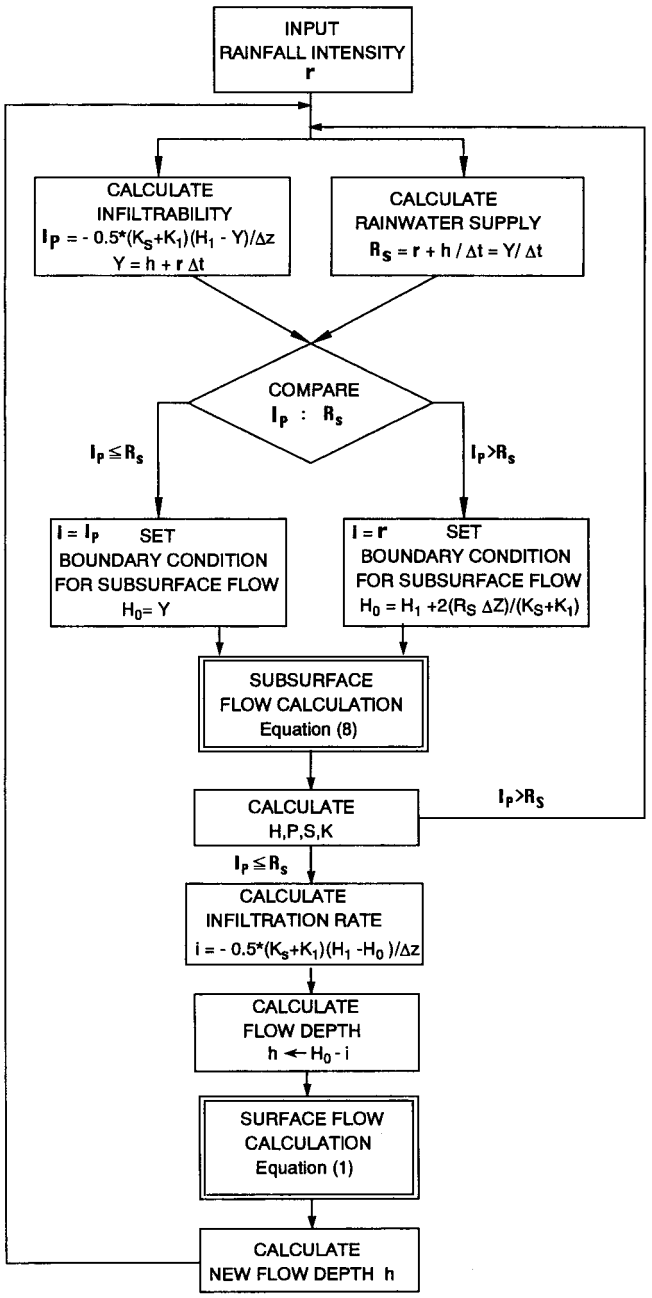

Figure 3. Flow chart of surface–sub-surface flow conjunctive model calculation.

Equation (7) is a special case of completely linear form of Equation (6). In this case, the well-known stability criterion for the purely explicit method is theoretically introduced as

$$\xi_1 = \kappa[(\Delta x)^{-2} + (\Delta y)^{-2}]\Delta t < 0.5 \tag{13}$$

where κ is the diffusivity coefficient equivalent to D_x and D_y in Equation (1). For the two ADE methods and the ADI method, theoretical analyses showed that the methods are unconditionally stable for the linear two-dimensional heat diffusion equation [15,19,20]. The present study investigates the stability characteristics of the six numerical methods for the non-linear heat diffusion equation as in Equation (1).

The parameter ξ_1 in Equation (13) can be regarded here as a stability parameter to observe the stability and accuracy characteristics of the six numerical methods; although Equation (1) is non-linear and has changeable diffusivity coefficients, D_x and D_y. The values of D_x and D_y for κ in the criterion are set at $0.5\,\mathrm{m^2\,s^{-1}}$ from the relation $D_r t_r / x_r^2 = 1$ in Equation (6).

The six numerical methods (Table III) were applied to Equation (1) to calculate the discharges Q at the downstream end of the plot for comparison with the constant rain intensity. In the calculation, the Reynolds number was always less than 30 000 and the frictional resistance was calculated either from Equation (3) or from Equation (4). The initial flow depth was assumed to be 0.01 mm. Since the accuracy and stability of the calculated values depend on the relation between Δx, Δy and Δt used, several different values of Δt were used with two different values of $\Delta x/\Delta y$ in the calculation of the discharge.

Figures 4–6 show the relations between the relative error and time increment, stability parameter (Equation (13)), or calculation time. The best result was obtained from Saul'yev's downstream method with the relative error less than 10^{-4}. Table IV lists a comparison of the different numerical methods for the surface flow sub-model as a summary in terms of their stability and error.

Figure 4(a) shows that large time discretization Δt results in large error for all methods. As expected, for small Δt, the purely explicit method is excellent in accuracy as is Saul'yev's downstream method, followed by the ADI, ADE (Barakat and Clark), ADE (Larkin), and Saul'yev's upstream method. The purely explicit method, however, has a stability problem, which is widely known and is demonstrated in Figure 4(a) with ξ_1 greater than 0.5. The coefficient D described in Equation (2) changes in time and in space and it ranged from 0.04 to $0.65\,\mathrm{m^2\,s^{-1}}$ in space after 8 min of rainfall. Using the reference value of $0.5\,\mathrm{m^2\,s^{-1}}$ for D, almost the same stability criterion, $\xi_1 = D\Delta t[(\Delta x)^{-2} + (\Delta y)^{-2}] < 0.5$, is found as in Equation (13). Saul'yev's upstream method and ADI method also become unstable when ξ_1 is greater than 5.

In addition to accuracy and stability, the time of calculation is another criterion for method comparison. Figure 4(b) shows the variation of relative errors with the calculation time corresponding to the symbol points of the different time increments shown in Figure 4(a). The unit of calculation time, u, shown in the figure is particular to the workstation computer used for the study, a Sun Microsystems Spark Station 10. Calculation time of 1 u is practically equal to about 1 s.

A method that has both small relative error and small calculation time is considered an excellent method. Therefore, Saul'yev's downstream method is the best, as shown in Figure

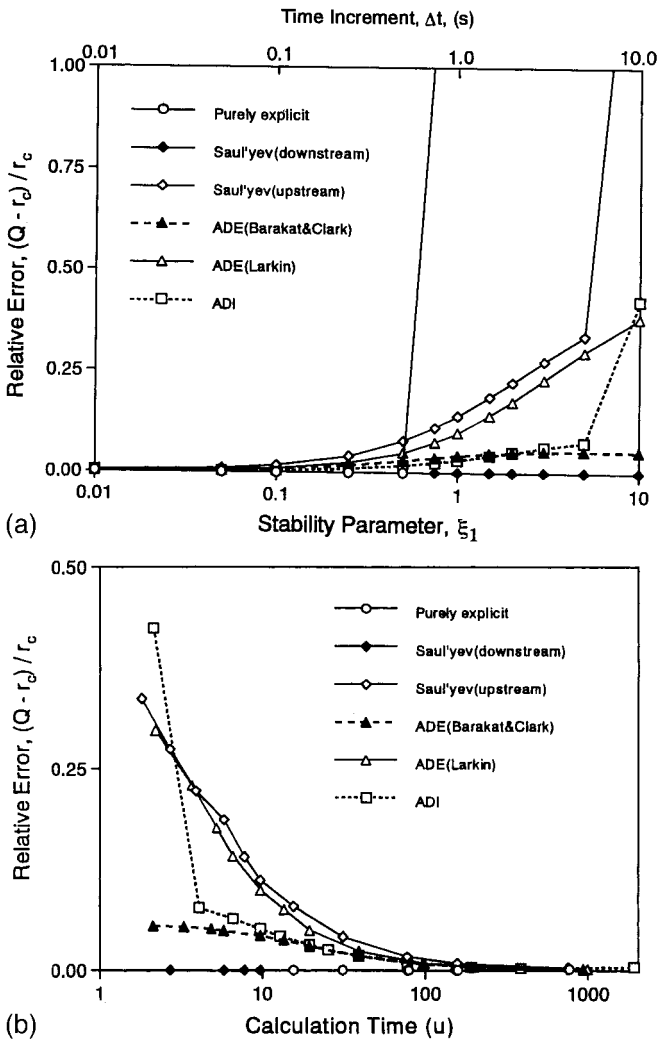

Figure 4. Relative error of surface flow simulation of Izzard's constant rain experiment titled 45° angle (Figure 2) for space increment, $\Delta x = \Delta y = 1.0$ m. (a) Relative error with stability parameter or time increment $\xi_1 = D[(\Delta x)^{-2} + (\Delta y)^{-2}]\Delta t$; $D = 0.5\ \mathrm{m^2\ s^{-1}}$, $\Delta x = \Delta y = 1.0$ m; (b) relative error with calculation time.

4(b). The purely explicit method needs a little more calculation time to give good results because of the small Δt required to control the stability problem. Likewise, Saul'yev's upstream method and Larkin's ADE method also need small Δt values and long calculation times to get good simulation results. Barakat and Clark's ADE method and the ADI method both yield reasonable results, whereas the former has been found slightly better than the latter in terms of relative error.

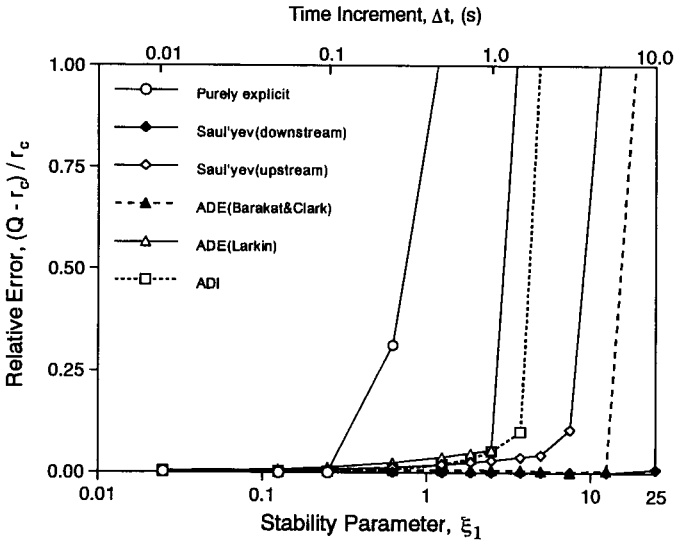

Figure 5. Relative error of surface flow simulation of Izzard's constant rain experiment titled 45° angle (Figure 2) for $\Delta x = 0.5$ m, $\Delta y = 1.0$ m $\xi_1 = D[(\Delta x)^{-2} + (\Delta y)^{-2}]\Delta t$; $D = 0.5\ \mathrm{m^2\,s^{-1}}$.

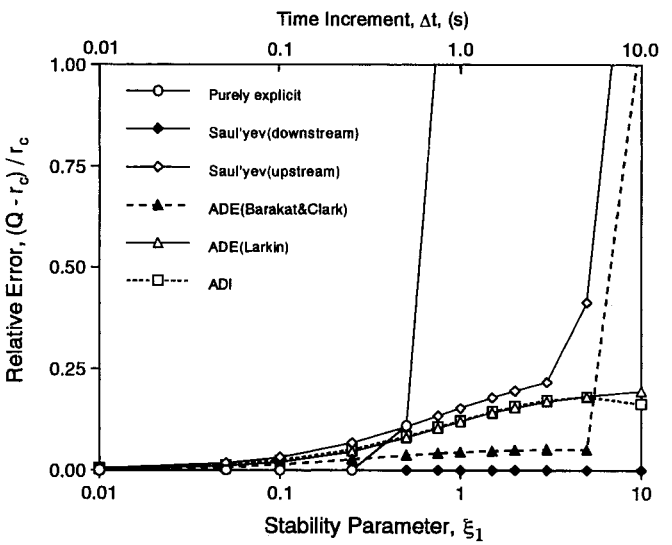

Figure 6. Relative error of surface flow simulation of Izzard's constant rain experiment titled 26.6° angle (Figure 2) for $\Delta x = \Delta y = 1.0$ m $\xi_1 = D[(\Delta x)^{-2} + (\Delta y)^{-2}]\Delta t$; $D = 0.5\ \mathrm{m^2\,s^{-1}}$.

Table IV. Comparison of different numerical methods for surface flow.

Method	Commencement of stability problem	Ranking of error	
		Small Δt	Large Δt
Saul'yev's downstream method	No	1	1
ADE method of Barakat and Clark	Large Δt ($\xi_1 > 10$)	4	2
ADI method	Mid Δt ($\xi_1 > 5$)	3	3
ADE method of Larkin	Mid Δt ($\Delta x \neq \Delta y$)	5	—
Saul'yev's upstream method	Mid Δt ($\xi_1 > 5$)	6	—
Purely explicit method	Small Δt ($\xi_1 > 0.5$)	1	—

In Figure 4(a) and (b), the spatial discretization ratio used is $\Delta x/\Delta y = 1$. To examine the effect of spatial discretization on the two-dimensional surface flow simulation, the ratio $\Delta x/\Delta y = 0.5$ is also tested for the condition of Izzard's experimental plot. The results are shown in Figure 5. The accuracies are slightly better than those in Figure 4(a) because of the smaller Δx. Each of the six methods has almost the same trend and similar stability criteria as in Figure 4(a), as theoretically expected. The purely explicit method becomes unstable with ξ_1 greater than 0.62. Barakat and Clark's ADE here is observed to be unstable with $\xi_1 > 12.5$.

The 45° tilting of Izzard's plot for two-dimensional simulation may not adequately reflect the problem in two-dimensional computations because of the diagonal symmetry of the x–y plane. Therefore, calculations were done with Izzard's plot tilted at a 26.6° angle (Figure 2), and the result as shown in Figure 6 is found to be almost the same as that in Figure 4(a). The ADE by Barakat and Clark becomes unstable as in Figure 5. The relative error of the ADI method becomes a little small at $\xi_1 = 10$. However, the calculation around $\xi_1 = 10$ is observed to be unstable.

5. VERIFICATION AND COMPARISON OF NUMERICAL METHODS FOR SUB-SURFACE FLOW MODEL

No analytical solution is available for non-linear two-dimensional and three-dimensional sub-surface flows to verify the numerical methods for the three-dimensional sub-surface flow model. Nor are experimental data that are sufficiently accurate and available. Therefore, in this study, a linearized analytical solution by Philip [25] for one-dimensional vertical downward percolation was applied for the verification. After the verification, the five numerical methods are evaluated for their stability and accuracy for three-dimensional sub-surface flow using reference bases to compare the numerical solutions. Both soil saturation profile and infiltration rate are evaluated.

5.1. One-dimensional downward flow and saturation degree profile

The linearized analytical solution (see Appendix A) by Philip [25] was applied for one-dimensional vertical percolation in the porous medium to verify and compare the five numerical methods. To obtain the analytical and numerical solutions, an idealized soil with the following hydraulic properties was assumed: $n = 0.125$; $\theta_0 = 0.025$ $(t = 0,\ z > 0)$, $\theta_1 = 0.125$ $(t > 0,\ z = 0)$, $S_0 = 0.2$, $S_1 = 1.0$, $K(\theta_0) = 1.25 \times 10^{-3}$ mm s^{-1}, $K(\theta_1) = 6.25 \times 10^{-3}$ mm s^{-1}. D^* and k in Philip's [25] analytical solution are constants having the following values:

$$D^* = K\frac{\mathrm{d}P}{\mathrm{d}\theta} = 2.5 \text{ mm}^2 \text{ s}^{-1} \tag{14}$$

$$k = \frac{\mathrm{d}K}{\mathrm{d}\theta} = \frac{1}{n}\frac{\mathrm{d}K}{\mathrm{d}S} = 0.05 \text{ mm s}^{-1} \tag{15}$$

In addition, the relation between P and S using Equations (14) and (15) was applied with the condition of $K_R = S$, resulting in

$$P = \frac{D^*}{k}\ln S \tag{16}$$

The P–S–K relation of the idealized soil used in the calculation is given in Figure 7.

For the numerical calculation, the values of the space increment and the number of grids in Figure 1 were set as follows: $\Delta x = \Delta y = \Delta z = 10$ mm; $N = M = 10$ and $L = 100$. The total number of the grids amounts to 10 000. The moisture diffusivity coefficient $\langle \alpha \rangle_{i,j,k}$ in Table II

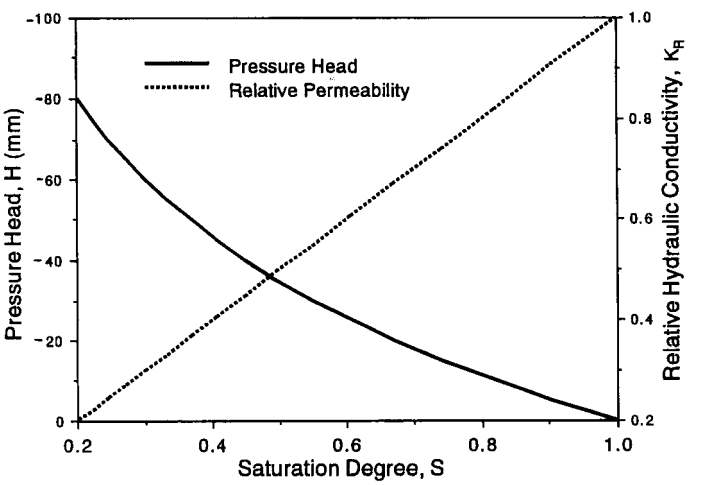

Figure 7. Hydraulic properties of soil used in calculation of Figure 8.

is set equal to the constant $D^* = 2.5\ \text{mm}^2\ \text{s}^{-1}$, but in the quasi-linear form of Equations (8) and (9), the soil hydraulic conductivity K changes with S and P as shown in Equations (14)–(16). After computing H in Equation (8) and P from the relation $P = H - z$, the values of saturation degree S can be obtained using Equation (16). Although the flow is actually one-dimensional, the calculation of Equation (8) was carried out three-dimensionally to compute the saturation degree S and the result was compared with Philip's one-dimensional analytical solution. For this calculation, the reference values in the non-dimensional equation (10) are set as follows: $x_r = y_r = z_r = 1.0$ m, $\alpha_r = D^* = 2.5\ \text{mm}^2\ \text{s}^{-1}$. The reference value of t_r is set at 400 000 s from the relation $\alpha_r t_r / x_r^2 = 1$ for simplification in Equation (10), which gives Equation (11). To observe the stability and accuracy, a stability parameter ξ_2 is also used here for three-dimensional sub-surface flow calculation in the same way as in Equation (13),

$$\xi_2 = \kappa[(\Delta x)^{-2} + (\Delta y)^{-2} + (\Delta z)^{-2}]\Delta t \tag{17}$$

where κ is the diffusivity coefficient equivalent to α or D^* in Equation (8). For the three-dimensional linear heat diffusion equation, the stability criterion of the purely explicit method is theoretically $\xi_2 < 0.5$.

Figure 8 shows the solution of Equations (8) or (10), together with Philip's analytical solution for the saturation degree at $t = 1000$ s and $t = 4000$ s respectively after the initiation of infiltration. It depicts the result obtained with the ADE method of Larkin using time increments $\Delta t = 10.0$ s for $t = 1000$ s and $\Delta t = 0.5$ s for $t = 4000$ s. The agreement between the two solutions is excellent. Larkin's ADE result is the best among the five numerical methods given in Table I; but the simulation results of the other four methods using the same Δt are almost the same, indistinguishable if plotted on the figure.

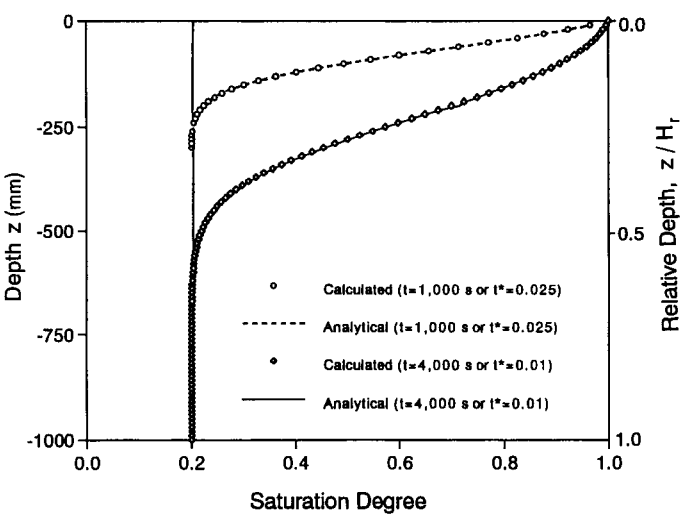

Figure 8. Comparison between calculated soil saturation by Larkin's ADE method with $\Delta t = 1.0$ s and Philip's analytical solution.

Similar to the case of the surface flow model, the accuracy, stability, and calculation time were investigated for the five numerical methods listed in Table I. The normalized error is calculated as

$$\delta_1 = \sqrt{\sum_{i=1}^{m} (S_i - S_{i0})^2/(m-1)} \Bigg/ \left(\sum_{i=1}^{m} S_{i0}/m \right) \tag{18}$$

where δ_1 is the normalized error; S_i is the degree of saturation for numerical solution; S_{i0} is the degree of saturation from the analytical solution; m is the number of saturation degrees.

Figure 9(a) shows the relation between normalized error and time increment Δt at $t = 1000$ s. The calculated saturation degrees used in Equation (18) are those from 0 to 0.3 m in depth. This is because the wetting front of infiltration at $t = 1000$ s ($t^* = 0.0025$) in Figure 8 exists around 0.3 m in depth. Similarly, the relation between the normalized error and time increment Δt at $t = 4000$ s ($t^* = 0.01$) is presented in Figure 9(b). For the calculation of Figure 9, α_{z1} and α_{z2} in Table II change with K, while $\alpha_{x1} = \alpha_{x2} = \alpha_{y1} = \alpha_{y2} = \alpha = \text{constant} = 2.5\ \text{mm}^2\ \text{s}^{-1}$. To calculate the normalized error, the values of saturation degree from 0 to 0.7 m in depth are used as indicated by the wetting front in Figure 8.

In Figure 9(a) the error increases with increasing time increment as in Figures 4(a), 5 and 6. For all the methods shown in Figure 9(a) or (b), the error becomes large for the stability parameter $\xi'_2 > 0.25$ ($\Delta t > 10$ s) where $\xi'_2 = \alpha \Delta t/(\Delta z)^2$. The purely explicit, Barakat and Clark's ADE, and the purely ADI methods have stability problems when ξ'_2 is larger than 0.25, 1.25 and 1.25 respectively. The observed critical values of the stability parameter $\xi'_2 = 0.25$ ($\Delta t = 10$ s) for the purely explicit method is a little smaller than in the linear case, $\xi'_2 = 0.5$. Unlike the two-dimensional surface flow sub-model, for quasi-linear three-dimensional sub-surface flow simulation the purely explicit method offers no advantage in accuracy, even for small Δt. The ADE method of Barakat and Clark is unstable for quasi-linear three-dimensional simulation. The three-dimensional purely ADI method is unstable as mentioned by Richtmyer and Morton [26]. In contrast, the ADE method of Larkin and the ADI method of Brian have been found stable and better than the other methods with the stability parameter less than 1.0. Beyond that, Brian's ADI method performs well. In Figure 9(b) the smallest errors for all of the numerical methods can be recognized as the time increment, ξ'_2, ranges from 0.01 to 0.025, where the normalized errors are found to be under 10^{-3}.

Figure 9(c) presents the relation between the normalized error and calculation time at $t = 4000$ s. Figures 9(c) and 10(b) are presented in the same way with the points related one to one to those of Figures 9(b) and 10(a) respectively. As mentioned previously, the unit of calculation time u is computer specific and in this study 1 u is roughly 1 s. Figure 9(c) shows that longer calculation time gives better results up to about 10 000 u. Beyond that calculation time the accuracy for the two ADE and the two ADI methods all decreases. Decreasing accuracy with longer calculation time is also found in the results of the three-dimensional heat diffusion calculation by Thibault [14] and can be explained by the accumulation of round-off errors in calculation with a large number of operations.

In the calculations of Figure 9, identical space increments of Δx, Δy and Δz were used. To examine the three-dimensional sub-surface flow simulation with different spatial discretization, $\Delta z = 5$ mm instead of 10 mm was used for otherwise the same sub-surface flow conditions as

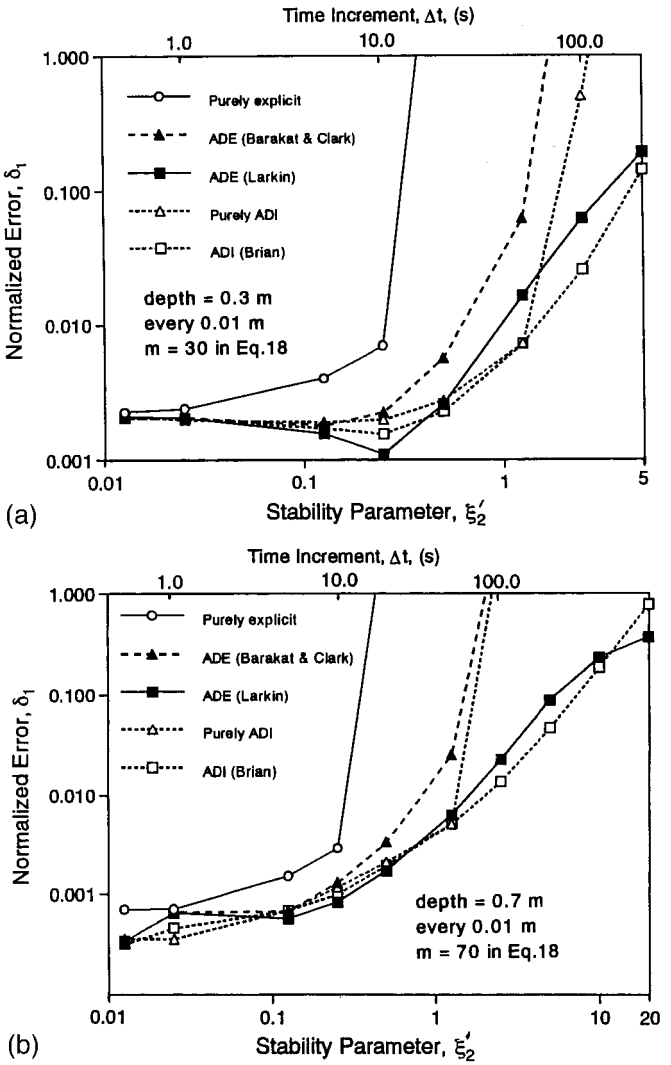

Figure 9. Normalized error of saturation degree (Equation (18)) for three-dimensional simulation of one-dimensional sub-surface flow under Philip's linearized condition, $\alpha = D^* = 2.5\ \text{mm}^2\ \text{s}^{-1}$. (a) Normalized error with stability parameter or time increment for saturation profile at $t = 1000$ s ($t^* = 0.0025$) $\xi'_2 = \alpha(\Delta z)^{-2}\Delta t$; $\alpha = 2.5\ \text{mm}^2\ \text{s}^{-1}$, $\Delta x = \Delta y = \Delta z = 10$ mm; (b) Normalized error with stability parameter or time increment for saturation profile at $t = 4000$ s ($t^* = 0.01$) $\xi'_2 = \alpha(\Delta z)^{-2}\Delta t$; $\alpha = 2.5\ \text{mm}^2\ \text{s}^{-1}$, $\Delta x = \Delta y = \Delta z = 10$ mm; (c) Normalized error with calculation time for saturation profile at $t = 4000$ s ($t^* = 0.01$), $\alpha = 2.5\ \text{mm}^2\ \text{s}^{-1}$, $\Delta x = \Delta y = \Delta z = 10$ mm; (d) Normalized error with stability parameter or time increment for saturation profile at $t = 4000$ s ($t^* = 0.01$) $\xi'_2 = \alpha(\Delta z)^{-2}\Delta t$; $\alpha = 2.5\ \text{mm}^2\ \text{s}^{-1}$, $\Delta x = \Delta y = 10$ mm, $\Delta z = 5$ mm.

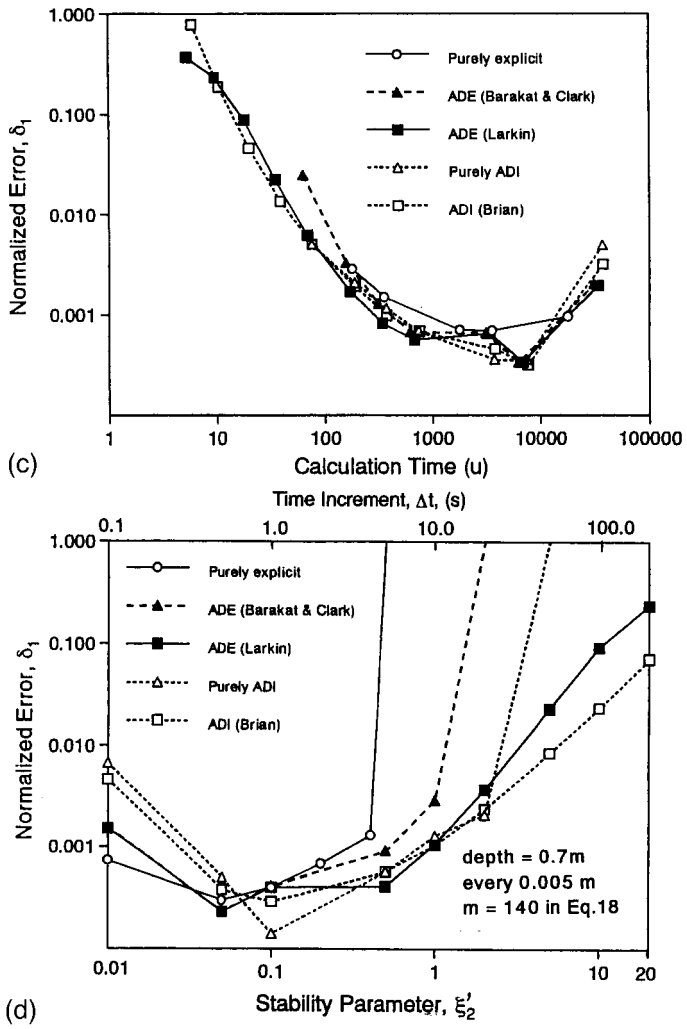

Figure 9 (*Continued*)

in Figure 9(b) and the results at $t = 4000$ s ($t^* = 0.01$) are shown in Figure 9(d). In general, the smaller space increment Δz improves accuracy. Each of the methods in Figure 9(d) have almost the same stability criteria as in Figure 9(b); the critical values of stability parameter for the purely explicit, Barakat and Clark's ADE, and the purely ADI methods are $\xi'_2 = 0.4$, 1.0 and 2.0 respectively. The ranking of the five different numerical methods based on the above discussion is summarized in Table V.

Table V. Comparison of different numerical methods for sub-surface flow.

Method	Commencement of stability problem	Ranking of error	
		Small Δt	Large Δt
ADE method of Larkin	No	1	2
ADI method of Brian	No	2	1
Purely ADI method	Large Δt ($\xi'_2 > 1.25$)	3	—
ADE method of Barakat and Clark	Large Δt ($\xi'_2 > 1.25$)	4	—
Purely explicit method	Small Δt ($\xi'_2 > 0.25$)	5	—

A number of previous studies on numerical methods compared the numerical solutions of the heat diffusion equation with analytical solutions. However, most of these studies dealt with a completely linear heat diffusion equation with constant diffusivity coefficients [14]. In the present study, the linearized equation of Philip [25] for which the hydraulic conductivity K in the equation varies with saturation degree as shown in Figure 7 is used. For a comparison of the completely linear diffusion equation with the numerical solution of the linearized equation of Philip, Figure 10(a) and (b) show the saturation degree at $t = 4000$ s on the condition that K is kept at a constant value of $0.0625\ \mathrm{mm\ s^{-1}}$ and moisture diffusivity $\alpha = D^* = 2.5\ \mathrm{mm^2\ s^{-1}}$. This means k in Equation (15) is equal to zero.

Figure 10(a) indicates that for the linear three-dimensional heat diffusion equation the purely explicit method is the most accurate among the methods until stability problems occur. This is different from the result for the one-dimensional quasi-linear case shown in Figure 9(a) and 9(b), and is similar to the two-dimensional surface flow shown in Figures 4(a) and 5. The observed stability criterion of the purely explicit method is, as in Equation (17), $\xi'_2 = \alpha(\Delta z)^{-2}\Delta t < 0.5$. This confirms that the sub-surface flow in the complete linear case of Figure 10 is one-dimensional, although the model calculation is carried out three-dimensionally. The normalized error reaches as low as 10^{-4}, which is on the same order as the case in Figure 9(b). The purely ADI method is also unstable when ξ'_2 is greater than 1.25. The other three methods, ADI of Brian and two ADEs, are numerically stable within the range tested. As in Figure 9(c), decreasing accuracy with longer calculation time beyond 100 u is observed in Figure 10(b). In Figure 10(a), the two ADI methods and the purely explicit method are better than the two ADE methods for time increment ξ'_2 smaller than 0.25, whereas Brian's ADI method is more accurate for ξ'_2 larger than 1.25. For the two ADE methods, Barakat and Clark's ADE method is stable and more accurate than Larkin's ADE method as mentioned by Anderson *et al.* [15]. The results of the three-dimensional linear case are in agreement with those of Thibault [14] and Anderson *et al.* [15]. In this comparison it is important to recognize that the numerical methods have different accuracy and stability characteristics between in the Philip's linearized case of Figure 9(a) and (b) and in the completely linear case of Figure 10(a).

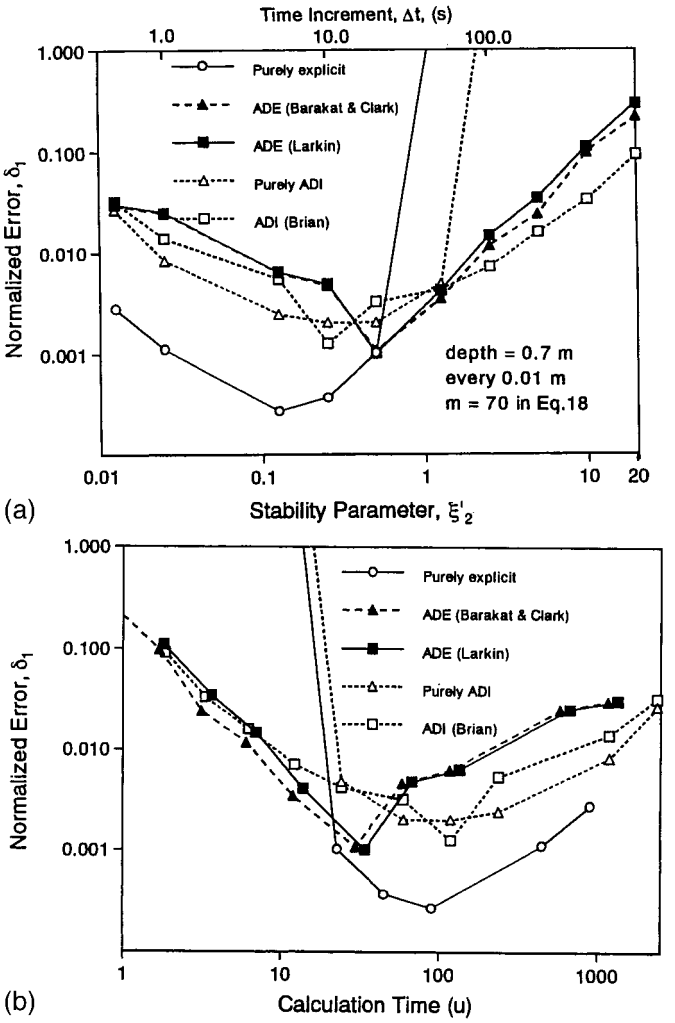

Figure 10. Normalized error of saturation degree (Equation (18)) for three-dimensional simulation of one-dimensional sub-surface flow with constant hydraulic conductivity, $K = 0.0625$ mm s^{-1}, $(\partial\theta/\partial P) = 0.025$ mm^{-1}, $\alpha = D^* = 2.5$ mm^2 s^{-1} . (a) Normalized error with stability parameter or time increment for saturation profile at $t = 4000$ s ($t^* = 0.01$) $\xi'_2 = \alpha(\Delta z)^{-2}\Delta t$; $\alpha = 2.5$ mm^2 s^{-1}, $\Delta x = \Delta y = \Delta z = 10$ mm; (b) (b) Normalized error with calculation time for saturation profile at $t = 4000$ s ($t^* = 0.01$).

5.2. Three-dimensional cross-directional percolation flow

The five numerical methods (Table I) are further examined for their application to the proposed sub-surface flow model for simulation of three-dimensional sub-surface percolation flows. With no analytical solutions nor sufficiently accurate experimental data for

three-dimensional sub-surface flow available as reference, certain values calculated by using a specified numerical method with a specified time increment are used as reference bases to compare the three-dimensional sub-surface flow simulations of the five numerical methods.

In this study, the linearized case of Philip calculated using Larkin's ADE method with $\Delta t = 10.0$ s, which shows the least error in Figure 9(a), is selected as the reference to compare the numerical methods for three-dimensional flow simulation. The soil properties and initial and boundary conditions used for this reference base are identical with those used to obtain Figures 9 and 10, i.e. Equations (14) and (15) and those given just preceding these equations. However, the values of the space increment and the number of grids in Figure 1 are set as $\Delta x = \Delta y = \Delta z = 10$ mm, and $N = M = 40$ and $L = 100$. The number of the grids totals to 160 000. The calculated reference of one-dimensional linearized saturation profile at $t = 1000$ s is plotted as the left curve in Figure 11.

The three-dimensional cross-directional sub-surface flows were calculated after the one-dimensional percolation simulation was established. The soil properties, initial condition, space increment, and the number of grids in Figure 1 were set as the same as in the one-dimensional percolation reference. The boundary conditions, however, were different; $\theta = 0.125$, $S = 1.0$ ($t > 0$, $x = 0$, $y = 0$ and $z = 0$), $\theta = 0.025$, $S = 0.2$ ($t > 0$, $x = 400$ mm, $y = 400$ mm and $z = 1000$ mm). Under these conditions, the sub-surface flow propagates in x-, y- and z-directions simultaneously, roughly from point A towards point G in Figure 1. The three curves to the right in Figure 11 are the three-dimensional flow saturation profiles in the z-direction at 1000 s at points $x = y = 50$ mm, $x = y = 100$ mm and $x = y = 150$ mm respectively. The curves were calculated from Larkin's ADE method with $\Delta t = 10.0$ s on Philip's linearized

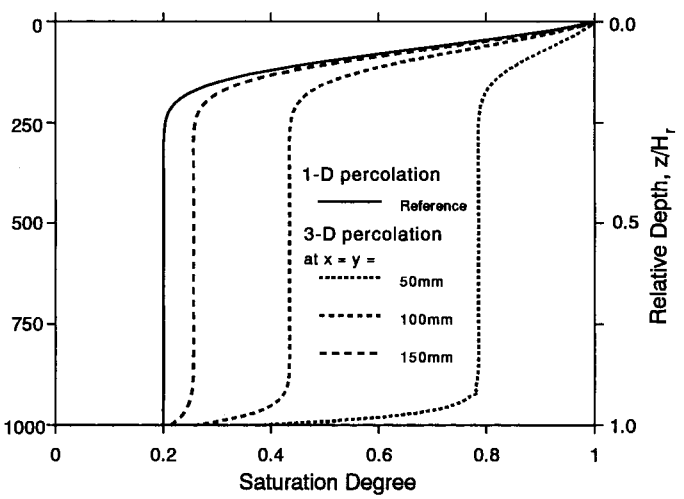

Figure 11. Calculated degree of soil saturation at $t = 1000$ s for three-dimensional and one-dimensional percolation by applying Larkin's ADE method to linearized three-dimensional equation of Philip, $\Delta t = 10$ s $\Delta x = \Delta y = \Delta z = 10$ mm.

three-dimensional sub-surface flow equation. The saturation degree of the three-dimensional percolation is larger than that of the one-dimensional percolation; it clearly decreases with increasing x, y and z, i.e. further from the source, as expected.

Figure 12 shows the relation between the normalized difference at $t = 1000$ s and time increment Δt in the calculation of three-dimensional sub-surface flow. The normalized difference between the calculated saturation profile of the three-dimensional flow and that of the reference three-dimensional percolation is computed as

$$\delta_2 = \sqrt{\sum_i \sum_j \sum_k (S_{i,j,k} - S^0_{i,j,k})^2/(m-1)} \Big/ \left(\sum_i \sum_j \sum_k S^0_{i,j,k}/m \right) \tag{19}$$

where δ_2 is the normalized difference; $S_{i,j,k}$ is the degree of saturation from numerical solution; $S^0_{i,j,k}$ is the degree of saturation from reference bases; m is the number of points of saturation degree. The saturation degrees calculated by Larkin's ADE method with $\Delta t = 10$ s for $S(i, j, k)$ ($i = 1$–40, $j = 1$–40, $k = 1$–100) in Figure 1 were adopted as reference bases $S^0_{i,j,k}$ for the examination. The number of the grids used for calculation with Equation (19) amounts to 160 000.

The numerical testing of the five methods for three-dimensional sub-surface flow, as illustrated in Figure 12, indicates that their stability and accuracy characteristics are almost the same as for one-dimensional flow shown in Figures 9 and 10. The ADE method of Larkin and the ADI method of Brian are stable and relatively accurate. The purely explicit method

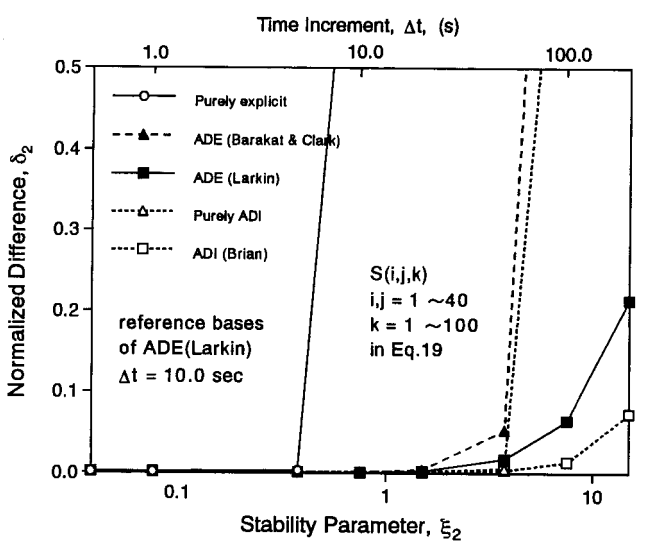

Figure 12. Comparison of normalized difference of saturation degree of sub-surface flow at $t = 1000$ s ($t^* = 0.0025$) calculated by using different numerical methods, $\xi_2 = \alpha[(\Delta x)^{-2} + (\Delta y)^{-2} + (\Delta z)^{-2}]\Delta t$, $\alpha = D^* = 2.5$ mm^2 s^{-1}, $\Delta x = \Delta y = \Delta z = 10$ mm.

becomes unstable when $\xi_2 > 0.5$. The purely ADI and ADE of Barakat and Clark become unstable at larger ξ_2.

5.3. Surface infiltration rate

The numerical solution of the time rate of infiltration through the ground surface can be calculated with Equation (12). Figure 13 presents the comparison of the surface infiltration rate between the numerical and analytical solutions. The numerical solution was obtained from the ADE method of Larkin with a time increment of 10 s. The numerical values agree with the analytical ones fairly well except during the first 50 s.

Similar to the case of the soil-saturation degree profile, the accuracy, stability and calculation time of the five numerical methods were investigated. The equation for the normalized error is

$$\delta_3 = \sqrt{\sum_{j=1}^{m} (i_j - i_{j0})^2/(m-1)} \Big/ \left(\sum_{j=1}^{m} i_{j0}/m \right) \tag{20}$$

where δ_3 is the normalized error; i_j is the numerically calculated surface infiltration rate at time j; i_{j0} is the analytically calculated surface infiltration rate at time j; m is the number of infiltration rates.

Figure 14(a) shows the relation between the normalized error and time increment for the five numerical methods investigated, in which the values of i were calculated every 20 s from 20 to 400 s, i.e. $m = 20$ in Equation (20). The ADE method of Barakat and Clark, ADE method of

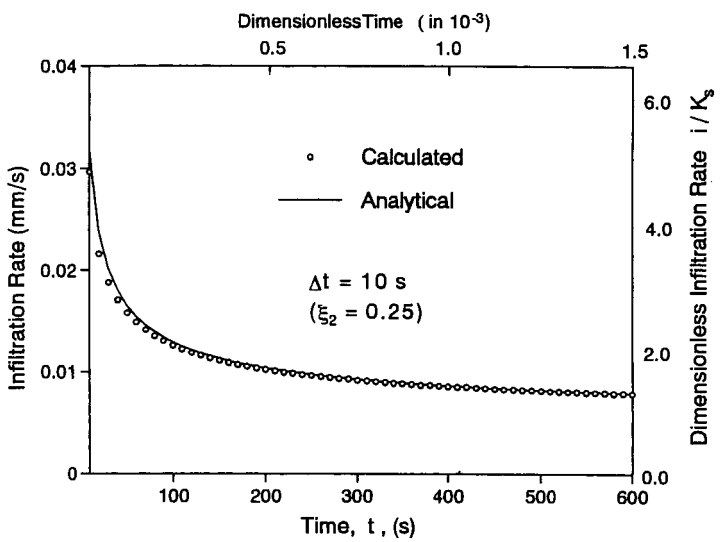

Figure 13. Comparison between infiltration rate calculated using ACE method of Larkin and Philip's analytical solution.

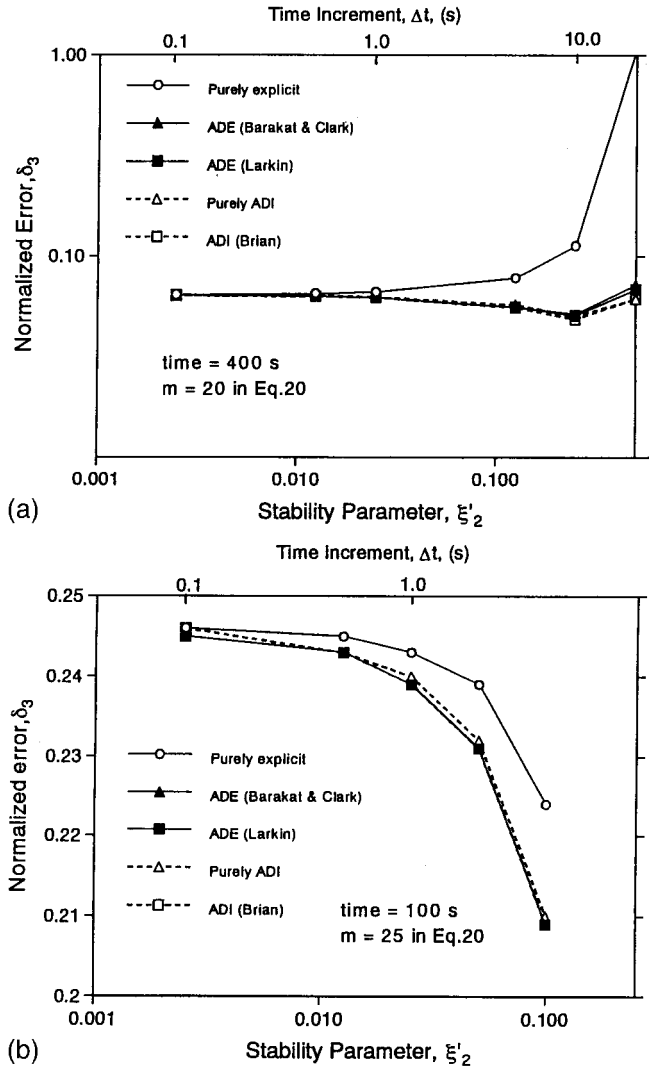

Figure 14. Normalized error (Equation (20)) of simulated infiltration rate into sub-surface with $\Delta x = \Delta y = \Delta z = 10$ mm $\xi'_2 = \alpha(\Delta z)^{-2}$; $\alpha = 2.5$ mm^2 s^{-1}. (a) Normalized error with stability parameter or time increment for first 400 s ($t^* = 0.001$); (b) Normalized error with stability parameter or time increment for first 100 s ($t^* = 0.0025$).

Larkin, ADI method of Brian, and the purely ADI method have almost the same accuracy. The curves for the two ADE methods are almost indistinguishable, as are the two ADI method curves. The purely explicit method is the least accurate of the methods tested. As shown in Figure 13, the agreement between the numerical and analytical values is not good in the first

50 s. To compare the numerical methods in detail for the early period, the values of i were calculated every 4 s, from 4 to 100 s ($m = 25$ in Equation (20)) and the results are shown in Figure 14(b). The normalized errors in Figure 14(b) are about four times larger than those in Figure 14(a). The ADE method of Barakat and Clark, the ADE method of Larkin, and the ADI method of Brian are better than the other methods shown in Figure 14(b).

The comparison among the numerical results of the different methods and with the analytical solutions as shown in Figures 9–14 facilitated the evaluation of the five numerical methods in terms of accuracy, stability, and calculation time. Larkin's ADE method and ADI method of Brian are unconditionally stable and more accurate than the other methods for three-dimensional simulations; i.e. different from the case of non-linear two-dimensional surface flow simulation shown in Figures 4–6, where Larkin's ADE method is less accurate and unstable. The ADE method of Barakat and Clark, the purely ADI method, and the purely explicit method have stability problems. The purely explicit method, however, has the advantage of easy and simple programming and gave almost the same accuracy as the ADE method of Larkin when using an appropriate small time increment with the stability parameter, ξ'_2, smaller than 0.5 in a linear and 0.25 in a linearized calculations respectively. Contrary to the three-dimensional quasi-linear simulation, Barakat and Clark's ADE method is slightly better than Larkin's ADE method for two-dimensional non-linear surface modeling (Figures 4 and 6) and three-dimensional linear (Figure 10) simulation.

6. DISCUSSION ON NUMERICAL CALCULATION OF THE CONJUNCTIVE MODEL

A numerical check of the conjunctive model that couples surface and sub-surface flow components was conducted after the numerical methods were tested for the surface and sub-surface flow models separately. The conjunctive model was first confirmed to produce a reasonable result under a given rainfall, and then the response of the numerical calculation to different time increments was examined as was done to verify separately the surface and sub-surface flow models.

Four surface flow numerical methods and three sub-surface flow numerical methods were used for the conjunctive models as listed in Table VI. From the testing of the saturation degree profile calculation of the sub-surface flow methods described in Section 5, the ADE method of Larkin and the ADI method of Brian have been found to be better than the other three methods listed in Table I. However, to couple the surface and sub-surface flow components, the surface infiltration rate as the common boundary condition is more important than the saturation profile. As described previously, testing of the surface infiltration rate of the sub-surface flow models (Figures 10(a) and 14) indicate that when Δt is not large the accuracy of the ADE method of Barakat and Clark is almost as good as the ADE method of Larkin and the ADI method of Brian. Hence, these three methods were applied for the three-dimensional sub-surface flow simulation in the conjunctive models: Model 1, Model 2 and Model 3 (Table VI). Each sub-surface flow sub-model was combined with four two-dimensional surface flow sub-models to examine the error interaction between the surface and sub-surface sub-models. Referring to Table IV, Saul'yev's downstream is the obvious choice of the surface

Table VI. Combination of surface and sub-surface flow models for conjunctive model calculation.

Conjunctive model	Sub-surface flow model	Surface flow model
Model 1	ADE method (Larkin)	Purely explicit method Saul'yev's method (downstream) Saul'yev's method (upstream) ADE method (Larkin)
Model 2	ADI method (Brian)	Purely explicit method Saul'yev's method (downstream) Saul'yev's method (upstream) ADE method (Larkin)
Model 3	ADE method (Barakat and Clark)	Purely explicit method Saul'yev's method (downstream) Saul'yev's method (upstream) ADE method (Larkin)

flow method. By considering the accuracy and stability shown in Figures 4–6, three other methods were also selected for testing. They are the purely explicit, Larkin's ADE, and Saul'yev's upstream. The number of combination totals to 12 as shown in Table VI.

For the numerical calculation of the coupled model, the values of the space increments and the number of grids for sub-surface flow in Figure 1 were set as follows: $\Delta x = \Delta y = 1.0$ m, $\Delta z = 10$ mm; $N = 10$, $M = 10$ and $L = 100$. The plane ABCD in Figure 1 is regarded as the surface for the calculation of Equation (1). The surface has the same Δx and Δy and slopes of 0.001 in the x- and y-directions as the case in Figure 2.

For the discretization condition described above, a typical simulation result of Model 1 for the surface and sub-surface flows (Saul'yev's downstream method for the surface flow and Larkin's ADE method for the sub-surface flow) is shown in Figure 15 for a triangular rainfall input. In the calculation, the discharge at the end of the surface CD (Figure 1), the average infiltration rate i over the whole surface ABCD, and the saturation degree in the soil layer were calculated under a spatially uniform rainfall with a triangular time distribution as shown in the figure. The boundaries AB, AD, and BC were closed without water flowing through. Soil properties were given in the same way as for the verification of the sub-surface flow models. The values of D^* and k in Equations (14) and (15) and the initial condition of S were set the same as those in the verification of the sub-surface flow models: $D^* = \alpha = 2.5\ \mathrm{mm^2\ s^{-1}}$, $k = 0.05\ \mathrm{mm^2\ s^{-1}}$ and $S = 0.2$ $(t = 0,\ z > 0)$. The relation shown in Figure 15 confirms the reasonableness of the conjunctive model calculation as will be mentioned.

Before testing the 12 conjunctive modeling options, the three models, Model 1, Model 2 and Model 3, each with Saul'yev's downstream method for surface flow were compared from the viewpoint of reasonableness of the conjunctive model simulation. The steady state discharge and infiltration rate were calculated for a spatially uniform rainfall with constant rainfall intensity of $150\ \mathrm{mm\ h^{-1}}$ for 20 min. When the runoff and infiltration reach the equilibrium stage at $t = 1200$ s, the discharge Q_c plus surface infiltration rate $\bar{i}_c$ is equal to the rainfall intensity r_c on the basis of water balance. In this checking calculation, Models 1, 2 and 3 were

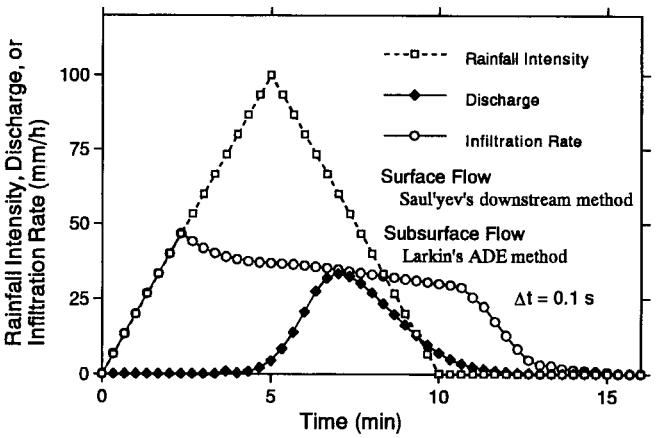

Figure 15. Results of conjunctive model calculation.

set to have the same soil saturation degree at the ponding time ($t = 0$ s) just before the overland flow starts and it is used as the initial condition. The comparison is made for different time increments as listed in Table VII. The relative errors of the three models are found to be under 10^{-3} for $\Delta t = 0.1$ s. The relative errors of the models are almost the same and increase linearly with time increment. Table VII shows that Model 3 with Barakat and Clark's ADE method for the sub-surface flow becomes unstable with $\Delta t = 30$ s. This stability problem of Barakat and

Table VII. Discharge (Q_c), surface infiltration rate (i_c) and relative error (ε_R) of the conjunctive model calculation by three models based on water balance at $t = 1200$ s measured from the time of overland flow initiation for constant rainfall intensity $r_c = 150$ mm h^{-1}, $\varepsilon_R = (Q_c + i_c - r_c)/r_c$.

Time increment (s)	0.1			1.0		
	Q_c	i_c	ε_R	Q_c	i_c	ε_R
Model 1	119.77	30.15	−0.00053	120.09	30.17	0.0018
Model 2	123.02	26.89	−0.00056	123.41	26.90	0.0020
Model 3	116.83	33.09	−0.00050	117.14	33.10	0.0016

Time increment (s)	20.0			30.0		
	Q_c	i_c	ε_R	Q_c	i_c	ε_R
Model 1	128.06	30.53	0.057	133.20	30.50	0.091
Model 2	132.61	26.82	0.063	138.15	26.73	0.099
Model 3	124.88	33.24	0.054	Unstable	Unstable	Unstable

Clark's ADE method for sub-surface flow calculation was mentioned for Figure 9(a) and (b). On the other hand, Model 1 with Larkin's ADE and Model 2 with Brian's ADI method remain stable with increasing time increment and the former is a little more accurate than the latter. From the checking calculation, Model 1 with Saul'yev's downstream method for surface flow and Larkin's ADE method for sub-surface flow was found to be the best for accuracy and stability. The result of Table VII, together with that of Figure 15, also confirm the reasonableness of the conjunctive model calculations for Models 1, 2 and 3.

To compare the three conjunctive models listed in Table VI, the errors of discharge Q and infiltration rate $\bar{i}$ calculated by the models with different Δt were investigated. For comparison purpose a reference basis of Q and $\bar{i}$ should be selected. Here the reference bases, Q_0 and $\bar{i}_0$, are taken to be the simulation results of Q and i with $\Delta t = 0.1$ s. The errors are calculated as the differences between this reference and the computed Q and using different Δt, i.e. $\varepsilon_a = Q - Q_0$ and $\varepsilon_b = \bar{i} - \bar{i}_0$. In this example calculation with triangular rainfall input as in Figure 15, we used the values of the discharge and infiltration rate at $t_p = 260$ s from the initiation of overland flow for Model 1, Model 2 and Model 3 when the peak discharge occurs, Q_p, Q_{p0} and the corresponding $\bar{i}$ and $\bar{i}_0$.

Figure 16(a) shows the variation of errors ε_a and ε_b with time increment for Model 1 for the example with triangular rain input. The values of the errors ε_b in infiltration rate are all positive and increase with Δt. The positive error of ε_b in infiltration rate results in negative error in the surface flow calculation. For surface flow modeling, the Saul'yev downstream method is the best and has the smallest positive error as shown in Figures 4–6. In Figure 16(a), the discharge error ε_a of Model 1 with Saul'yev's downstream method for surface flow is negative and grows gradually with Δt. This can be explained by the direct effect of the sub-surface flow calculation on the discharge error just described. On the other hand, in the calculation of Model 1 with the other three methods for surface flow, the positive error effect of surface flow calculated by the methods overwhelms the negative error effect of the sub-surface flow component. This results in rapidly increasing positive error with Δt as shown in Figure 16(a). In particular, for Model 1 with purely explicit method the discharge calculation becomes unstable with $\Delta t > 2$ s. As described in the verification of surface flow modeling the purely explicit method is unstable with Δt greater than 0.5 s as shown in Figures 4–6. In the conjunctive model calculation, the effect of negative error in the sub-surface flow calculation reduces the conjunctive accumulation of error and hence the stability lasts longer than in surface flow calculation alone.

Thus, Figure 16(a) indicates that in conjunctive modeling the contribution to the infiltration error ε_b from the sub-surface flow calculation with the ADE method of Larkin is also influenced by the numerical method applied in the surface flow calculation. Model 1 with Saul'yev's downstream method for surface flow has the least error in infiltration rate. Model 1 with the purely explicit method yields the worst results and has stability problems whereas errors of Model 1 with Larkin's ADE or Saul'yev's upstream are in between.

Figure 16(b) shows the variation of errors with time increment for Model 2. Almost the same trend is observed in Figure 16(b) as in Figure 16(a). For the option of purely explicit scheme for surface flow, not only the discharge but also the surface infiltration rate becomes unstable with Δt larger than 2.0 s.

For Model 3 the variation of the discharge error with time increment shown in Figure 16(c) is a little different from that for Model 1 or Model 2. The error of the surface infiltration rate calculated from Model 3 with Saul'yev's downstream method for surface flow is found to be negative, whereas the other errors of the surface infiltration rate in Figure 16(a)–(c) are all positive. The negative error of surface infiltration rate causes the positive error of the discharge

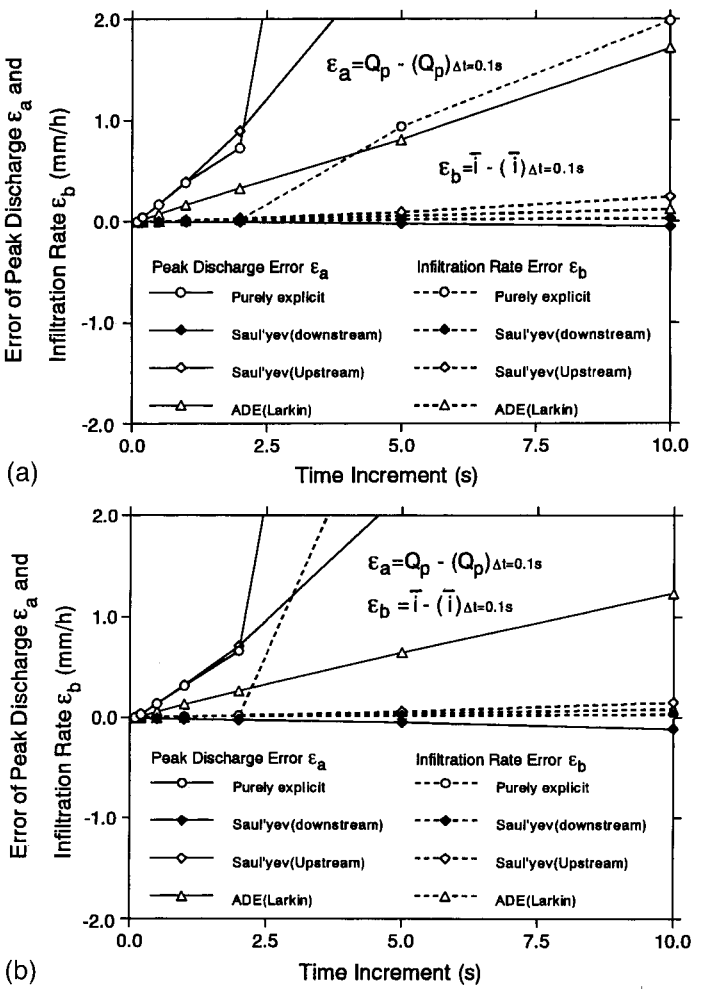

Figure 16. Relation between time increment and coupled modeling error of peak discharge and surface infiltration rate. (a) Error of peak discharge and infiltration rate with time increment for Model 1 (Larkin's ADE method for sub-surface flow model); (b) Error of peak discharge and infiltration rate with time increment for Model 2 (Brian's ADI method for sub-surface flow model); (c) Error of peak discharge and infiltration rate with time increment for Model 3 (Barakat and Clark's ADE for sub-surface flow model).

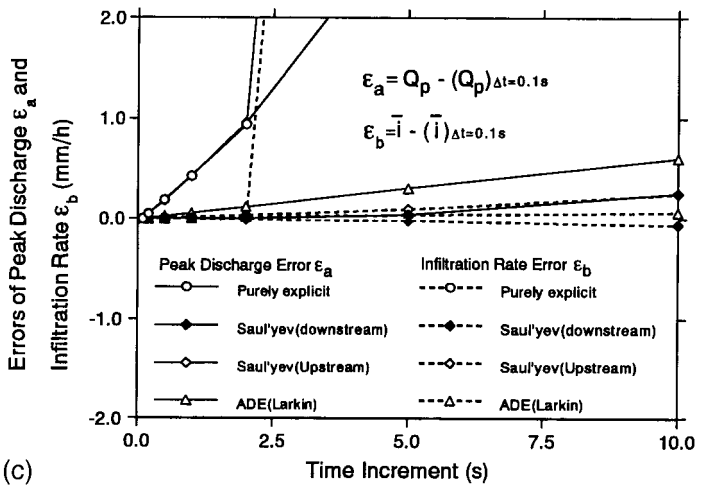

Figure 16 (*Continued*)

calculated by Model 3 with Saul'yev's downstream method as clearly shown in Figure 16(c). This result further confirms the interaction between surface and sub-surface flow calculations.

It is difficult to generalize quantitatively the error structure here. However, the interaction between the errors in surface flow calculation and those in the sub-surface flow calculation is easily seen in the conjunctive model results. The characteristics of this interaction are a subject worthy of further study in the future. The errors of the infiltration rate, ε_b, are smaller than those of the discharge, ε_a, from the comparison shown in Figure 16(a)–(c). From the results of the conjunctive model calculations in Figure 16(a)–(c), the surface flow option of Saul'yev's downstream method is clearly superior to the other three options. The best coupling of surface and sub-surface flow components is the combination of Saul'yev's downstream method for surface flow and Larkin's ADE method for sub-surface flow because of its smallest error with increasing time increment and its shorter calculation time.

Figure 16(a)–(c) also show that the surface flow calculation dominates the stability and accuracy in the conjunctive model calculation. Over 80 per cent of the total calculation time was spent in the sub-surface model calculation. Therefore, which numerical method to choose for sub-surface flow dominates the total calculation time for the conjunctive model.

7. CONCLUDING REMARKS

The comparison and verification of the six numerical methods for the surface flow model presented in this paper yielded several concluding remarks as follows:

(1) All of the numerical methods tested resulted in fairly good agreement between the calculated and observed data provided an appropriate time increment ($\xi_1 < 0.1$; $\xi_1 = D[(\Delta x)^{-2} + (\Delta y)^{-2}]\Delta t$, $D = 0.5\,\mathrm{m^2\,s^{-2}}$) is used.

(2) The purely explicit method and Saul'yev's downstream method gives the best results in terms of accuracy with relative errors under 10^{-3}.

(3) Saul'yev's downstream method is the best in the overall comparison. This method gives excellent results in the case of two-dimensional calculations such as that shown in Figure 2. The ADE method of Barakat and Clark is the preferred alternatives considering stability, relative error and calculation time.

(4) The purely explicit method gives good results, but it has stability problems for large time increments. If a small time increment ($\xi_1 < 0.5$; $\xi_1 = D[(\Delta x)^{-2} + (\Delta y)^{-2}]\Delta t$, $D = 0.5\ \mathrm{m^2\ s^{-1}}$) is used to avoid the stability problem, this method could be the best.

For the sub-surface flow model, five numerical methods were verified and compared. The concluding remarks are

(5) Solutions of all the numerical methods for the profile of saturation degree and for the infiltration rate agree well with Philip's analytical solution of the one-dimensional linearized sub-surface flow equation.

(6) Larkin's ADE and Brian's ADI methods are unconditionally stable and more accurate than the other methods. With a stability parameter ξ'_2 ($\xi'_2 = \alpha(\Delta z)^{-2}\Delta t$, $\alpha = 2.5\ \mathrm{mm^2\ s^{-1}}$) smaller than 1.0, the former is more accurate and vice versa with a larger stability parameter $\xi'_2 > 1.0$. In terms of accuracy and calculation time, Larkin's ADE method is slightly better than Brian's ADI method.

(7) The examination of the five numerical methods for three-dimensional percolation indicates that the stability and accuracy characteristics of the methods are almost the same as for one-dimensional percolation.

(8) The purely explicit method is the most accurate one until stability problems occurs as demonstrated in the calculation of a special, completely linear case with constant hydraulic conductivity.

(9) The purely explicit method, the ADE method of Barakat and Clark, and the purely ADI method all have stability problems in quasi-linear three-dimensional numerical solutions when ξ_2 ($\xi_2 = \alpha[(\Delta x)^{-2} + (\Delta y)^{-2} + (\Delta z)^{-2}]\Delta t$, $\alpha = 2.5\ \mathrm{mm^2\ s^{-1}}$) is larger than 0.5, 5 and 5 respectively.

(10) The ADE method of Larkin and the ADI method of Brian are unconditionally stable and more accurate than the other methods tested. These two are the preferred methods for three-dimensional sub-surface flow modeling.

After separate verification and comparison of the numerical methods for the surface flow and sub-surface flow sub-models, three conjunctive models were investigated. For sub-surface flow model, three methods were applied: Larkin's ADE, Brian's ADI, and Barakat and Clark's ADE methods. Each method was combined with four methods for surface flow model: Saul'yev's downstream and upstream, Larkin's ADE, and purely explicit methods. The number of combination totals 12. It has been found that

(11) The errors of surface flow and sub-surface flow sub-models interact not only the magnitudes but also the signs (positive or negative) of both errors have an effect on the error of the conjunctive model.

(12) The surface flow sub-model dominates the accuracy and stability of the conjunctive model because the surface flow sub-model errors are larger than those of the sub-surface flow sub-model with the same time increment.

(13) The sub-surface flow sub-model dominates the total calculation time of the conjunctive model. Therefore, a larger time increment for the sub-surface flow sub-model than for the surface flow model could be used to save calculation time with the same accuracy.

(14) For conjunctive surface and sub-surface flow modeling, the surface flow option of Saul'yev's downstream method is clearly superior to the other three options: Larkin's ADE, Saul'yev's upstream, and purely explicit methods in this order.

(15) Among the 12 conjunctive modeling options tested, the best coupling of surface and sub-surface flow components is the combination of Saul'yev's downstream method for surface flow and Larkin's ADE method for sub-surface flow because of its smallest error with increasing time increment and its shorter calculation time. This finding is further supported by conclusion items (3), (6) and (10).

APPENDIX A

The equation for percolation in a semi-infinite, homogeneous, one-dimensional soil system of uniform initial moisture content is described in the linearized form as follows:

$$\frac{\partial\theta}{\partial t} = D^* \frac{\partial^2\theta}{\partial z^2} - k\frac{\partial\theta}{\partial z} \tag{A1}$$

$$D^* = K\frac{\mathrm{d}P}{\mathrm{d}\theta} = \text{constant} \tag{A2}$$

$$k = \frac{\mathrm{d}K}{\mathrm{d}\theta} = \frac{K(\theta_1) - K(\theta_0)}{\theta_1 - \theta_0} = \text{constant} \tag{A3}$$

$$t = 0; \quad z > 0, \quad \theta = \theta_0 \tag{A4}$$

$$t \geq 0; \quad z = 0, \quad \theta = \theta_1 \tag{A5}$$

where θ is the moisture content; $K(\theta)$ is the unsaturated hydraulic conductivity; P is the capillary pressure. Equations (A4) and (A5) are the initial and boundary conditions respectively.

The analytical solution of this equation was obtained by Philip [25]

$$\theta = \theta_0 + \frac{\theta_1 - \theta_0}{2}\left[\mathrm{erfc}\left(-\frac{z - kt}{2(D^*t)^{1/2}}\right) + \exp\left(\frac{kz}{D^*}\right)\mathrm{erfc}\left(-\frac{z + kt}{2(D^*t)^{1/2}}\right)\right] \tag{A6}$$

The infiltration rate was also solved as

$$i = -K_0 + D^*\left[\frac{(\theta_1 - \theta_0)}{(\pi D^* t)^{1/2}}\exp\left(-\frac{k^2 t}{4D^*}\right) - \frac{(\theta_1 - \theta_0)}{2}\frac{k}{D^*}\,\mathrm{erfc}\left(-\frac{kt^{1/2}}{2(D^*)^{1/2}}\right)\right] \tag{A7}$$

where K_0 is the hydraulic conductivity at the soil surface.

REFERENCES

1. Freeze RA. Role of subsurface flow in generating surface runoff: 1. Base flow contribution to channel flow. *Water Resources Research* 1972; **8**(3): 609–623.
2. Liggett JA, Dillon PJ. *A dynamic model of flow exchange between streams and aquifers*. Proceedings of IAHR 21st Congress, Melbourne, Australia, vol. 1, 1985; 17–22.
3. Yen BC, Riggins R. *Time scales for conjunctive modeling of subsurface and surface water motion*. Irrigation and Drainage, Proceedings of ASCE National Conference, Honolulu, 1991; 351–358.
4. Smith RE, Woolhiser DA. Overland flow on an infiltration surface. *Water Resources Research* 1971; **7**(4): 899–913.
5. Katopodes ND, Strelkoff T. Hydrodynamics of border irrigation: complete model. *Journal of the Irrigation and Drainage Division, ASCE* 1977; **103**(IR3): 309–323.
6. Playan E, Walker WR, Merkley GP. Two-dimensional simulation of basin irrigation, 1: theory. *Journal of Irrigation and Drainage Engineering, ASCE* 1994; **120**(5): 837–856.
7. Savabi MR. Modeling subsurface drainage and surface runoff with WEPP. *Journal of Irrigation and Drainage Engineering, ASCE* 1993; **119**(5): 801–813.
8. SinghV, Bhallamudi SM. Complete hydrodynamic border-strip irrigation model. *Journal of Irrigation and Drainage Engineering, ASCE* 1996; **122**(4): 189–197.
9. Pinder GF, Sauer SP. Numerical simulation of flow wave modification due to back storage effects. *Water Resources Research* 1971; **7**(1): 63–70.
10. Akan AO, Yen BC. Mathematical model of shallow water flow over porous media. *Journal of the Hydraulics Division, ASCE* 1981; **107**(HY4): 479–494.
11. Schmitz G, Haverkamp R, Palacios VO. *A coupled surface–subsurface model for shallow water flow over initially dry soil*. Proceedings of 21st IAHR Congress, Melbourne, Australia, vol. 1, 1985; 23–30.
12. Yen BC. Hydraulic resistance in open channels. In *Channel Resistance: Centennial of Manning's Formula*, Yen BC (ed). Water Resources Publications: Highlands Ranch, CO, 1991; 15.
13. Hellums JD, Churchill SW. Simplification of the mathematical description of boundary and initial value problems. *American Institute of Chemical Engineering Journal* 1964; **10**(1): 110–114.
14. Thibault J. Comparison of nine three-dimensional numerical methods for the solution of the heat diffusion equation. *Numerical Heat Transfer* 1985; **8**: 281–298.
15. Anderson DA, Tannehill JC, Pretcher RD. *Computational Fluid Mechanics and Heat Transfer*. Taylor & Francis: Bristol, 1985; 115–120.
16. Wong YS, Hafez MM. Conjugate gradient methods applied to transonic finite difference and finite element calculations. *AIAA Journal* 1982; **20**: 1526–1533.
17. Jameson A, Yoon S. Multigrid solution of the Euler equations using implicit schemes. *AIAA Journal* 1986; **24**: 1737–1743.
18. Jameson A. Transonic aerofoil calculations using the euler equations. In *Numerical Methods in Aeronautical Fluid Dynamics*, Roe PL (ed). Academic Press: New York, 1982.
19. Barakat HZ, Clark JA. On the solution of the diffusion equation by numerical methods. *Journal of Heat Transfer* 1966; **88**: 421–427.
20. Larkin BK. Some stable explicit difference approximation to the diffusion equation. *Mathematics of Computer* 1964; **18**: 196–202.
21. Brian PLT. A finite-difference method of high-order accuracy for the solution of three-dimensional transient heat conduction problems. *American Insitiute of Chemical Engineering Journal* 1961; **7**(3): 367–370.
22. Saul'yev VK. *Integration of Equations of Parabolic Type by the Method of Nets*. Macmillan: New York, 1964; 116–118.
23. Peaceman RD, Rachford HH Jr. The numerical solution of parabolic and elliptic differential equations. *Journal of Society Industrial Applied Mathematics* 1955; **3**: 28–41.
24. Izzard CF. Hydraulics of runoff from developed surfaces. *Proceedings, Highway Research Board* 1946; **26**: 129–146.
25. Philip JR. Theory of infiltration. In *Advances in Hydroscience*, vol. 5, Chow VT (ed). Academic Press: New York, 1969; 216–295.
26. Richtmyer RD, Morton KW. *Difference Methods for Initial-Value Problems*, 2nd edn. Wiley-Interscience: New York, 1967; 212–216.

